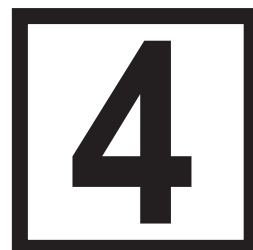
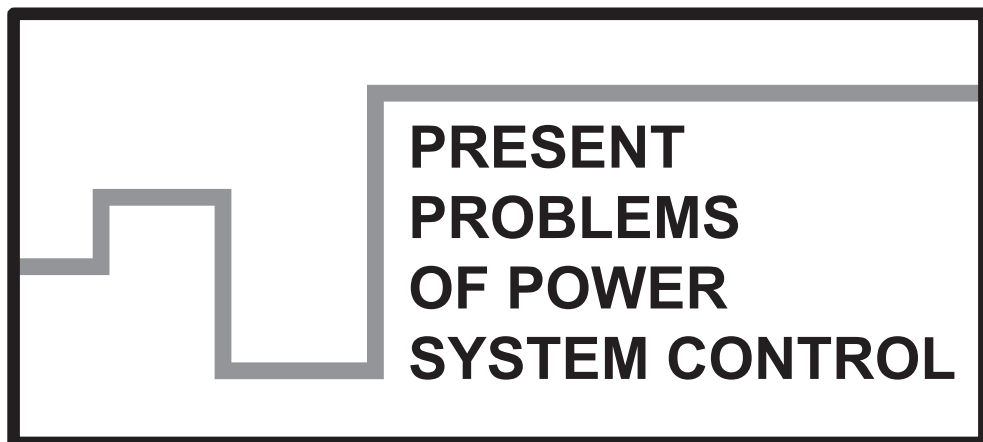


**Scientific Papers of
the Institute of Electrical Power Engineering of
the Wrocław University of Technology**



Wrocław 2013

Guest Reviewers

Ivan DUDURYCH
Tahir LAZIMOV
Murari M. SAHA

Editorial Board

Piotr PIERZ – art manager
Mirosław ŁUKOWICZ, Jan IŻYKOWSKI, Eugeniusz ROSOŁOWSKI,
Janusz SZAFRAN, Waldemar REBIZANT, Daniel BEJMERT

Cover design

Piotr PIERZ

Printed in the camera ready form

Institute of Electrical Power Engineering
Wrocław University of Technology
Wybrzeże Wyspiańskiego 27, 50-370 Wrocław, Poland
phone: +48 71 320 26 55, fax: +48 71 320 26 56
www: <http://www.ie.pwr.wroc.pl/>; e-mail: Inst.Energ@pwr.wroc.pl

All right reserved. No part of this book may be reproduced by any means, electronic, photocopying or otherwise, without the prior permission in writing of the Publisher.

© Copyright by Oficyna Wydawnicza Politechniki Wrocławskiej, Wrocław 2013

OFICYNA WYDAWNICZA POLITECHNIKI WROCŁAWSKIEJ
Wybrzeże Wyspiańskiego 27, 50-370 Wrocław
<http://www.oficyna.pwr.wroc.pl>
e-mail: oficwyd@pwr.wroc.pl
zamawianie.ksiazek@pwr.wroc.pl

ISSN 2084-2201

Drukarnia Oficyny Wydawniczej Politechniki Wrocławskiej. Order No. 706/2013.

CONTENTS

R. G. FERRAZ, L. U. IURINIC, A. D. FILOMENA, A. S. BRETAS, Park's Transformation Based Formulation for Power System Transients Detection	5
B. BRUSIŁOWICZ, J. SZAFRAN, Influence of Transformer Tap Changer Operation on Voltage Stability	25
M. PUSTUŁKA, J. IŻYKOWSKI, M. ŁUKOWICZ, Neural Network Filtration for Arc Faults Location on Power Transmission Lines	37
P. SAWKO, K. HILL, G. EVANS, Design and Testing of Power System Protection Functions Using Simulink [®] and EMTP	51
T. LAZIMOV, E. SAAFAN, Transitional Processes at Switching-off Unloaded Power Transmission Lines by Modern Circuit-Breakers and Their Computer Simulation	67

Renato Gonçalves FERRAZ*, Leonardo Ulises IURINIC*,
André Darós FILOMENA*, Arturo Suman BRETAS*

PARK'S TRANSFORMATION BASED FORMULATION FOR POWER SYSTEMS TRANSIENTS DETECTION

This paper presents proposed developments of a new formulation and a full algorithm for transient detection by applying Park's transformation. This approach consist in transforming three-phase voltage or current signals into Park's components known as direct, quadrature, and zero axes components. The input signals are local measurements of a power transmission or distribution system. Then, transients are superimposed in three-phase signals that can be detected in Park's components through the finite difference between samples. A full algorithm for the transient detection is presented and envisions the possibility of being applied in real time. In order to demonstrate the proposed algorithm's performance, four case studies are considered: *capacitor energizing*, *distribution transformer energizing*, *permanent resistive fault*, and *high impedance fault*. These cases were simulated on a typical Brazilian sub-transmission line using Alternative Transient Program. As demonstrated by the case studies, the proposed formulation introduces further improvements for transient detection in power systems.

1. INTRODUCTION

It is well known that rapid changes in circuit states create electromagnetic transients seen in the system variables. The term transient indicates an event that is undesirable but only momentary in nature, disappearing during the transition from one steady state to another. Common sources of electromagnetic transients in power systems are lightnings, faults, and switching operations. They create impulsive or oscillatory transients that can affect the performance of equipment or damage their electrical insulation [1].

Transient waveforms contain frequency components besides the fundamental frequency that characterizes the phenomenon that produced the transient. In power sys-

* Electrical Engineering Department, Federal University of Rio Grande do Sul, Porto Alegre, Brazil.

tems, phenomena like faults are common and can cause, between others, system currents increase.

Detection of transients in power systems can initiate relay tripping or fault location methods. The correct detection is very important to determine the exact time when these phenomena began.

Many approaches are proposed in the literature to detect a transient or an abnormal system condition. The method application depends on the particular problem to be solved. The easiest to implement methods are based on sample-by-sample or cycle-by-cycle derivatives of currents or voltages signals. When this derivative overruns a pre-set value, an auxiliary counter starts to count. This counter is incremented by the absolute value of the derivative and confirms the event when it reaches another pre-set threshold [2].

Energy variations in a certain frequency band can be used as an indicator of anomalies in the system. Specific values of relative increase in harmonics can be used to detect the presence of a High Impedance Faults (HIF) or capacitor-bank switching [3]. Characteristics in the low frequency spectrum, given by 2nd and 3rd harmonics, can also be used to detect abnormal conditions produced by HIF [4]. These frequency methods can effectively detect the presence of transients by analyzing the frequency spectrum in a fixed sample window. Nonetheless, if time resolution is very poor they cannot provide with acceptable precision the beginning and end of the transient. Reference [5] shows a clear example of using Discrete Wavelet Transform (DWT) to detect transient events. The theory of wavelets filter banks is well presented and a high impedance fault can be distinguished from a capacitor-bank switching by analysis of the periodicity of the peaks. In [6] the imaginary part of the Morlet-type mother wavelet is used to create a band-pass filter with a central frequency determined by system parameters. A specific relation among ground voltage phases and currents is used to identify healthy feeders from one disturbed by a HIF. Wavelets can also be combined with singular value decomposition and Shannon entropy concepts creating a technique called Wavelet Singular Entropy (WSE) [7]. This technique basically indicates the complexity of an analyzed signal in the time-frequency domain. When a WSE increases above a particular threshold, the transient is detected and also classified by comparing the WSE of each phase. Sometimes it is preferred to detect or record only a specific type of event based on voltage measurements such as a voltage dip. Wavelet coefficients exactly points out the beginning and end of voltage dip exactly, but the high-frequency noise present are also detected. Thus, some classification criteria such as wavelet networks [8] or Kalman filter [9] must be used. In [10] an algorithm is presented for a fault location in transmission lines where the transient detection is based on the Park's transformation. However, this work does not present a theoretical approach about the transient detection through Park's transformation. An analytical study of Park's transformation contextualized on electric power system

transient assessment is presented in [11]. Nevertheless, this study is performed considering the transient signal in only one phase of a set of voltages signals.

Several state-of-the-art proposed techniques are interested in power systems linear faults and normal switching detection. High impedance faults detection however is still a major challenge. A generalized approach that contributes to the further improvement of new techniques for electromagnetic transient detection in power systems is the main goal of this paper. Considering this, a Park's transformation based formulation applied to three phase voltages signals is developed and presented. Following, the equations are analyzed in detail considering some important conditions of power systems. Finally, several examples of transient signals generated by faults and switching operations in electric power system are presented. These signals were generated by Alternative Transient Program (ATP) simulations and are used to exemplify the use of the proposed formulation performance.

2. PARK'S TRANSFORMATION: TRANSIENT DETECTION

Park's transformation relates variables defined in a static reference frame with variables defined in a rotating reference frame. The most known application of the transformation is in analysis of rotating electric machines, turning the variables inductances of the stator in constant inductances on a rotating reference with synchronous speed [12]. Figure 1 illustrates this application, where q -axis and d -axis are the quadrature and direct axes respectively, ω is the angular power frequency and θ is the angle between phase a and direct axes.

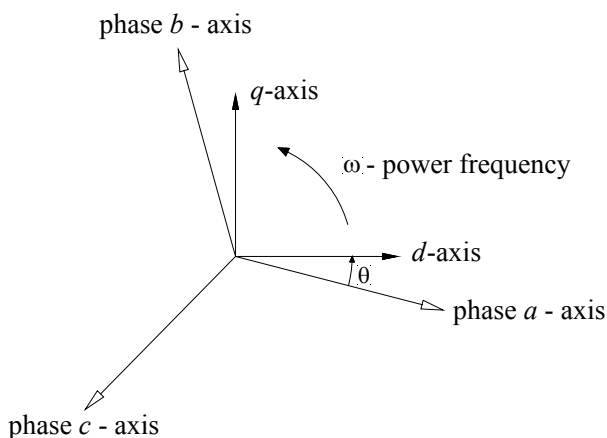


Fig. 1. Diagram of a three-phase system and dq components

Park's transformation matrix T_p can be expressed as [12]:

$$T_p = \sqrt{\frac{2}{3}} \begin{bmatrix} \cos(\omega t + \theta) & \cos(\omega t - \frac{2\pi}{3} + \theta) & \cos(\omega t + \frac{2\pi}{3} + \theta) \\ -\sin(\omega t + \theta) & -\sin(\omega t - \frac{2\pi}{3} + \theta) & -\sin(\omega t + \frac{2\pi}{3} + \theta) \\ \sqrt{\frac{1}{2}} & \sqrt{\frac{1}{2}} & \sqrt{\frac{1}{2}} \end{bmatrix} \quad (1)$$

where ω is the angular power frequency, t is the time instant, and θ is the angle between phase a and direct axes.

The method allows the transformation from the abc phases to the $dq0$ components in the following matrix form [12]:

$$V_{dq0} = T_p \cdot V_{abc} \quad (2)$$

where:

$V_{dq0} = [v_d \ v_q \ v_0]^T$ is the vector of signals $dq0$;

v_d , v_q , and v_0 are the components of direct, quadrature, and zero axes, respectively;

$V_{abc} = [v_a \ v_b \ v_c]^T$ is the vector of abc signals;

v_a , v_b , and v_c are the signals of the phases a , b , and c , respectively.

The detection of electromagnetic transients due to switching actions, energizing operations, faults, and lightning in a power system can be the initial process to differentiate between normal events and potentially damaging events. To demonstrate the property of the Park's transformation to detect transient signals in power systems, consider the following set of voltage signals from a three-phase system with electromagnetic transients in all phases as:

$$\begin{bmatrix} v_a \\ v_b \\ v_c \end{bmatrix} = \begin{bmatrix} V_{ma} \cos(\omega t) + f_a(t) \\ V_{mb} \cos(\omega t - 2\pi/3) + f_b(t) \\ V_{mc} \cos(\omega t + 2\pi/3) + f_c(t) \end{bmatrix} \quad (3)$$

where:

$f_a(t)$, $f_b(t)$, and $f_c(t)$ are the functions that represent the electromagnetic transient signal in phases a , b , and c , respectively;

V_{ma} , V_{mb} , and V_{mc} are the maximum values of signals of the phases a , b , and c , respectively.

Transients were considered in all phases because they are usually coupled. Therefore, an event in one phase is propagated to the others.

Park's transformation according to (2) is applied to (3) and after the application of some trigonometric identities [13], results in v_0 , v_d , and v_q components as:

$$v_0 = \sqrt{\frac{2}{3}} \cdot \sqrt{\frac{1}{2}} \left\{ \left[V_{ma} \cos(\omega t) + V_{mb} \cos\left(\omega t - \frac{2\pi}{3}\right) + V_{mc} \cos\left(\omega t + \frac{2\pi}{3}\right) \right] + [f_a(t) + f_b(t) + f_c(t)] \right\} \quad (4)$$

$$v_d = \sqrt{\frac{2}{3}} \cdot \left\{ \begin{aligned} & \left[\frac{1}{2}(V_{ma} + V_{mb} + V_{mc})\cos(\theta) + \right. \\ & \left. \left[\frac{1}{2}\left(V_{ma} - \frac{1}{2}V_{mb} - \frac{1}{2}V_{mc}\right)\cos(2\omega t + \theta) + \frac{\sqrt{3}}{2}(V_{mc} - V_{mb})\sin(2\omega t + \theta) \right] + \right. \\ & \left. \left[\left(f_a(t) - \frac{1}{2}f_b(t) - \frac{1}{2}f_c(t)\right)\cos(2\omega t + \theta) - \frac{\sqrt{3}}{2}(f_b(t) + f_c(t))\sin(\omega t + \theta) \right] \right\} \quad (5) \end{aligned} \right.$$

$$v_q = \sqrt{\frac{2}{3}} \cdot \left\{ \begin{aligned} & \left[\frac{1}{2}(V_{ma} + V_{mb} + V_{mc})\sin(\theta) + \right. \\ & \left. \left[\frac{1}{2}\left(V_{ma} - \frac{1}{2}V_{mb} - \frac{1}{2}V_{mc}\right)\sin(2\omega t + \theta) + \frac{\sqrt{3}}{2}(V_{mb} - V_{mc})\cos(2\omega t + \theta) \right] + \right. \\ & \left. \left[\left(f_a(t) - \frac{1}{2}f_b(t) - \frac{1}{2}f_c(t)\right)\sin(\omega t + \theta) + \frac{\sqrt{3}}{2}(f_c(t) + f_b(t))\cos(\omega t + \theta) \right] \right\} \quad (6) \end{aligned} \right.$$

Again applying trigonometric relationships [13] on (4), (5) and (6), the following expressions are obtained:

$$v_0 = k_1 \cos(\omega t - \delta_0) + \frac{\sqrt{3}}{2} [f_a(t) + f_b(t) + f_c(t)] \quad (7)$$

where:

$$k_1 = \sqrt{k_2^2 + k_3^2} \quad (8)$$

$$k_2 = \frac{\sqrt{3}}{3} \left(V_{ma} - \frac{1}{2}V_{mb} - \frac{1}{2}V_{mc} \right) \quad (9)$$

$$k_3 = \frac{1}{2} (V_{mb} - V_{mc}) \quad (10)$$

and

$$\delta_0 = \tan^{-1}(k_3 / k_2) \quad (11)$$

Similarly, (5) may be rewritten as:

$$v_d = \sqrt{\frac{2}{3}} [V \cos(\theta) + k_4 \cos(2\omega t + \theta - \delta) + m(t) \cos(\omega t + \theta - \delta_T(t))] \quad (12)$$

where:

$$V = \frac{1}{2}(V_{ma} + V_{mb} + V_{mc}) \quad (13)$$

$$k_4 = \sqrt{k_5^2 + k_6^2} \quad (14)$$

$$k_5 = \frac{1}{2} \left(V_{ma} - \frac{1}{2} V_{mb} - \frac{1}{2} V_{mc} \right) \quad (15)$$

$$k_6 = \frac{1}{2} \frac{\sqrt{3}}{2} (V_{mc} - V_{mb}) \quad (16)$$

$$\delta = \tan^{-1}(k_6 / k_5) \quad (17)$$

$$m(t) = \sqrt{m_1^2(t) + m_2^2(t)} \quad (18)$$

$$m_1(t) = f_a(t) - \frac{1}{2} f_b(t) - \frac{1}{2} f_c(t) \quad (19)$$

$$m_2(t) = \frac{\sqrt{3}}{2} [f_b(t) - f_c(t)] \quad (20)$$

and

$$\delta_T(t) = \tan^{-1}(m_2(t) / m_1(t)) \quad (21)$$

Likewise, (6) may be rewritten as:

$$v_q = \sqrt{\frac{2}{3}} [V \sin(\theta) + k_4 \sin(2\omega t + \theta - \delta) + m(t) \sin(\omega t + \theta - \delta_T(t))] \quad (22)$$

Thus, the application of Park's transformation on (3) results in:

$$\begin{bmatrix} v_0 \\ v_d \\ v_q \end{bmatrix} = \begin{bmatrix} k_1 \cos(\omega t - \delta_0) + \frac{\sqrt{3}}{3} [f_a(t) + f_b(t) + f_c(t)] \\ \sqrt{\frac{2}{3}} [V \cos(\theta) + k_4 \cos(2\omega t + \theta - \delta) + m(t) \cos(\omega t + \theta - \delta_T(t))] \\ -\sqrt{\frac{2}{3}} [V \sin(\theta) + k_4 \sin(2\omega t + \theta - \delta) + m(t) \sin(\omega t + \theta - \delta_T(t))] \end{bmatrix} \quad (23)$$

The relationship between v_d and v_q as orthogonal projections of the same vector can be explicitly seen in (23). Function $m(t)$ can be understood as composition point by point of functions $m_1(t)$ and $m_2(t)$ whose angle is $\delta_T(t)$. They only depend on the existence of transient signals superimposed with fundamentals ones. On the other hand, because parameters k_2 and k_3 depend only on the amplitude of fundamental components, it is possible to interpret them as components of a vector with angle δ_0 and modulus k_1 . The same can be said of the parameters k_5 and k_6 in relation to k_4 and angle δ . Angle θ , as shown in Fig. 1, is the angle between phase a and direct axes. It is a constant with a stochastic value depending on the moment when Park's transformation is applied. However, to simplify the presented analysis of v_0 , v_d and v_q components, this angle will be considered zero.

3. EQUATIONS ANALYSIS

This section will analyze the set of equations (23) from the perspective of important power systems operating conditions.

A. Balanced System Operating without Electromagnetic Transient

A balanced system operating in the absence of an electromagnetic transient is given as $V_{ma} = V_{mb} = V_{mc} = V_m$ and $f_a(t) = f_b(t) = f_c(t) = 0$. For these conditions and analyzing (23) it is possible to verify that:

$$v_0 = 0 \quad (24)$$

$$v_d = \sqrt{\frac{2}{3}} V \cos(\theta) = \frac{\sqrt{6}}{2} V_m \cos(\theta) \quad (25)$$

and

$$v_q = -\sqrt{\frac{2}{3}} V \sin(\theta) = -\frac{\sqrt{6}}{2} V_m \sin(\theta) \quad (26)$$

In other words, the application of Park's transformation to a set of signals at the fundamental frequency of a balanced system results only in a DC level of v_d , and v_q components that depends on angle θ .

B. Balanced System Operating with Electromagnetic Transient

A balanced system operating during the presence of an electromagnetic transient is given as $V_{ma} = V_{mb} = V_{mc} = V_m$ and $f_a(t)$, $f_b(t)$ and $f_c(t)$ with nonzero values. For these conditions and by analyzing (23) is possible to verify that:

$$v_0 = \frac{\sqrt{3}}{3} [f_a(t) + f_b(t) + f_c(t)] \quad (27)$$

$$v_d = \sqrt{\frac{2}{3}} [V \cos(\theta) + m(t) \cos(\omega t + \theta - \delta_T(t))] = \sqrt{\frac{2}{3}} \left[\frac{3}{2} V_m \cos(\theta) + m(t) \cos(\omega t + \theta - \delta_T(t)) \right] \quad (28)$$

and

$$v_q = -\sqrt{\frac{2}{3}} [V \sin(\theta) + m(t) \sin(\omega t + \theta - \delta_T(t))] = -\sqrt{\frac{2}{3}} \left[\frac{3}{2} V_m \sin(\theta) + m(t) \sin(\omega t + \theta - \delta_T(t)) \right] \quad (29)$$

That is, the application of Park's transformation to a set of signals at the fundamental frequency of a balanced system operating during the presence of electromagnetic transient results in:

- the sum of the transient signals for the v_0 component, multiplied by a constant;
- a constant plus a combination of transient signal term for the v_d and v_q .

C. Unbalanced System Operating without Electromagnetic Transient

An unbalanced system operating in the absence of an electromagnetic transient is given as $V_{ma} \neq V_{mb} \neq V_{mc}$ and $f_a(t) = f_b(t) = f_c(t) = 0$. For these conditions and by analyzing (23) it is possible to verify that:

$$v_0 = k_1 \cos(\omega t - \delta_0) \quad (30)$$

$$v_d = \sqrt{\frac{2}{3}} [V \cos(\theta) + k_4 \cos(2\omega t + \theta - \delta)] \quad (31)$$

and

$$v_q = -\sqrt{\frac{2}{3}} [V \sin(\theta) + k_4 \sin(2\omega t + \theta - \delta)] \quad (32)$$

The application of Park's transformation for the conditions described above results in:

- a cosine with fundamental frequency in v_0 component;
- a DC level plus a second harmonic in v_d and v_q component;

D. Unbalanced System Operating with Electromagnetic Transient

An unbalanced system operating during the presence of electromagnetic transient is given as $V_{ma} \neq V_{mb} \neq V_{mc}$ and $f_a(t), f_b(t)$ and $f_c(t)$ with nonzero values. For these conditions and by analyzing (23) is possible to verify that:

$$v_0 = k_1 \cos(\omega t - \delta_0) + \frac{\sqrt{3}}{3} [f_a(t) + f_b(t) + f_c(t)] \quad (33)$$

$$v_d = \sqrt{\frac{2}{3}} [V \cos(\theta) + k_4 \cos(2\omega t + \theta - \delta) + m(t) \cos(\omega t + \theta - \delta_T(t))] \quad (34)$$

and

$$v_q = -\sqrt{\frac{2}{3}} [V \sin(\theta) + k_4 \sin(2\omega t + \theta - \delta) + m(t) \sin(\omega t + \theta - \delta_T(t))] \quad (35)$$

In other words, the application of Park's transformation for the conditions described above results in:

- the v_0 component is a fundamental frequency and transient signals combination;
- the v_d and v_q components have the following combination:
 - DC level;
 - second harmonic of the fundamental frequency;
 - modified frequency and amplitude combination of transient signals.

At this point can be clearly verified that conditions described in items *A*, *B*, and *C* are particular cases of the condition described in *D*. For a better understanding of the Park's application, consider the following example.

F. Example

Consider a set of balanced voltages, all with an amplitude of 1 pu, with a momentary oscillatory transient in phase *a*. Such a transient signal is a signal whose energy is concentrated in certain ranges of time and frequency ranges. Such a signal may be mathematically represented by a Gaussian envelope, which is characterized in this example by a standard deviation of 2 ms, centered at 2.6 ms and modulated by a cosine function of 500 Hz according to:

$$f_a(t) = 0.5 \cdot e^{-\frac{1}{2} \left(\frac{t-0.026}{0.002} \right)^2} \cos(2\pi \cdot 500 \cdot t) \quad (36)$$

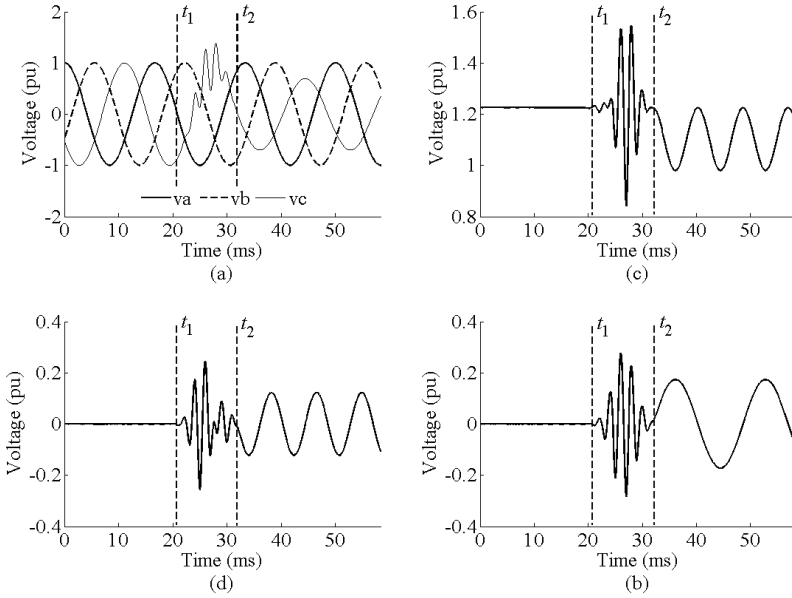


Fig. 2. Park's transformation: (a) phase voltages; (b) v_0 ; (c) v_d ; (d) v_q

Immediately before the occurrence of the transient at phase c , an unbalance was characterized by a voltage of phase c of 0.8 pu. As shown in Fig. 2, upon the beginning of the transient approximately in t_1 , v_0 signal is zero and v_d and v_q signals are constant values given by (25) and (26) respectively. Before t_1 , v_0 is proportional to the proper transient as shown in (27). The signals v_d and v_q are modified according to (28) and (29), not only by an amplitude modification but also by a frequency distortion. This distortion is given by multiplications of the transient component $m(t)$ with a sine and cosine. After the transient dies out at t_2 , an unbalance can be seen by the aspersion of a fundamental frequency term in v_0 and second harmonics in v_d and v_q .

4. TRANSIENTS DETECTION ALGORITHM AND CASE STUDIES

Using Park's transformation to detect transients allows supervision of the power systems three phases with only one signal and eliminates the fundamental frequency effect, improving the transient detection. It is possible to use any Park's component (v_0 , v_d or v_q) for detection approach, in this paper the v_d component is used.

The finite difference approximation of the derivate can be used in the v_d component for transient detection as follows:

$$c_{diff}(k) = v_d(k) - v_d(k-1) \quad (37)$$

where k is the sample number. The finite difference quantities concept is broadly used in the literature [14].

According to (31), if an unbalanced voltage condition is present an oscillation of twice the fundamental frequency in v_d is produced. This oscillation is also seen in c_{diff} and its amplitude is used as a threshold. To perform the transient detection, the square of c_{diff} is used as a way to attenuate noises and magnify transient components. In [10], c_{diff}^2 was used to attenuate noises and magnify transient components and the adaptive method was also proposed.

In order to have more control in the sensibility of the detection algorithm for the most important electromagnetic transients in power systems, a full algorithm and two threshold transient detections are presented. The basic idea is to count the times that c_{diff}^2 exceeds the adaptive threshold at some time interval. As was analyzed before in case *B* of section 3, in a case of unbalance, v_d will be composed of a second harmonic and a DC level as shown (31). As a result c_{diff} is composed only by a second harmonic. Then, the module of this second harmonic is used as the adaptive threshold. Figure 3 shows the steps of the proposed detection algorithm.

Figures 4 and 5 exemplify the algorithm showing the v_d signal, c_{diff}^2 and the adaptive threshold. The first sample of c_{diff}^2 due to a transient beginning is much larger than the threshold can be seen in Fig. 4. The second sample is below the threshold, but the four subsequent samples are above the threshold. For the five samples above the threshold before time count reached the value of time threshold, the transient is confirmed and detected. In Fig. 5 a short transient occurs and is seen in v_d 's signal, the first sample of c_{diff}^2 after the transient beginning is much larger than the threshold. On the other hand, because less than five samples are above the threshold before the time_count reaches the thime_threshold, the transient is not detected.

Aiming to demonstrate the proposed formulation performance, four case studies were considered: *capacitor energization*, *distribution transformer energization*, *permanent resistive fault*, and *high impedance fault*. These cases were simulated on a typical Brazilian sub-transmission line using ATP. The line is 30 km long and has a nominal voltage of 69 kV, it is connecting two substations in the state of Rio Grande do Sul. In order to simulate a situation closer to reality, also the phenomenon of travelling wave was also considered using a frequency dependent line model. Note that all stated cases are hypotheticals, only the line model is a reproduction of a real situation. For all cases is used a time_threshold of 10 and count_threshold of 5. Figure 6 shows the power system used in the case studies where the Digital Transient Recorder (DTR) is in the local terminal. The switches S_1 , S_2 , S_3 , and S_4 are closed individually for each case.

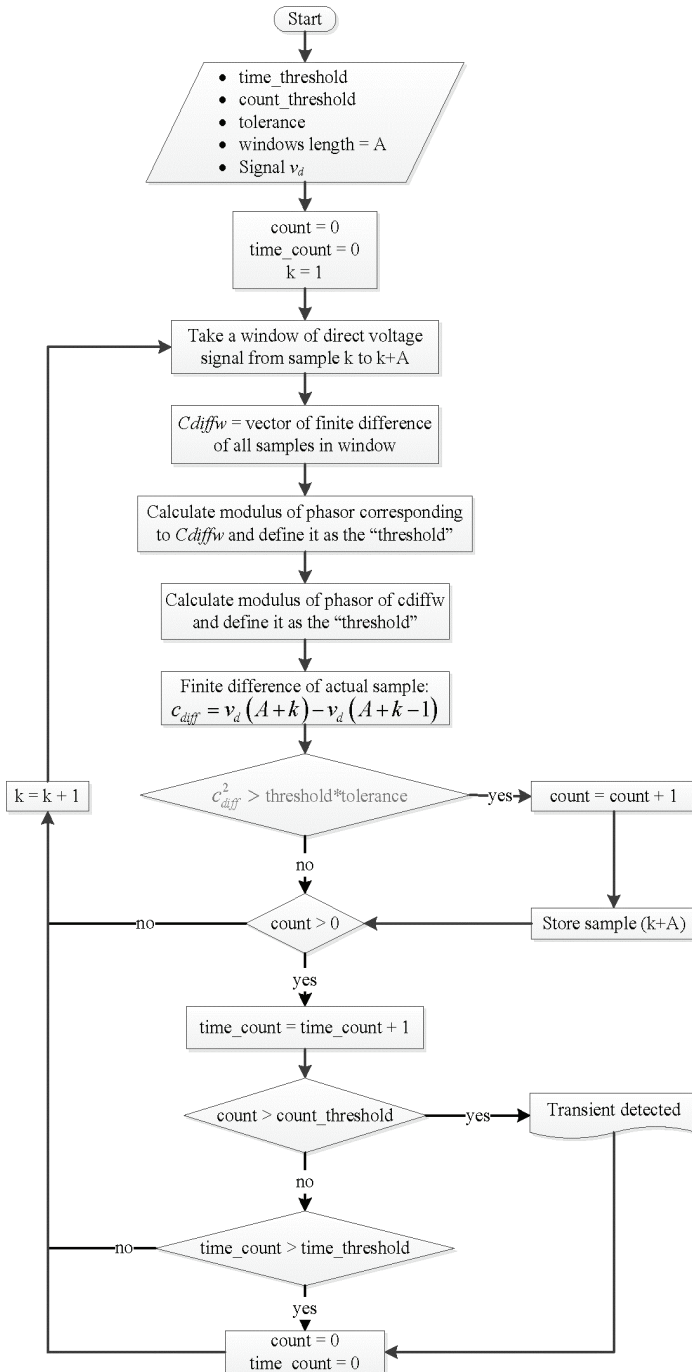


Fig. 3. Full algorithm for the transient detection

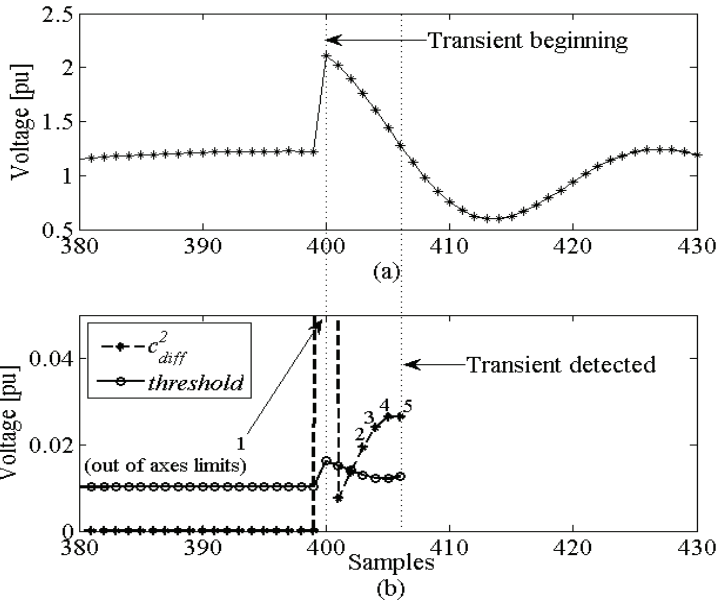


Fig. 4. Transient detection: (a) v_d component; (b) adaptive threshold

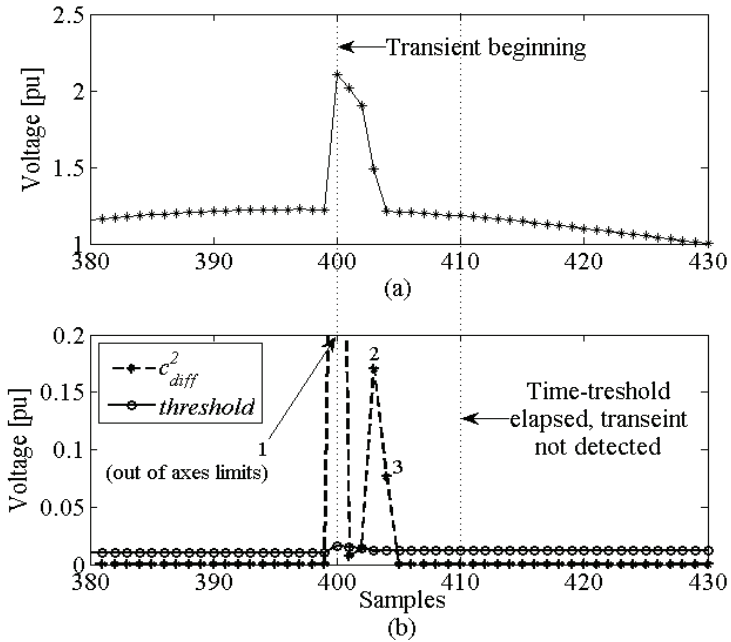


Fig. 5. Not transient detection: (a) v_d component; (b) adaptive threshold

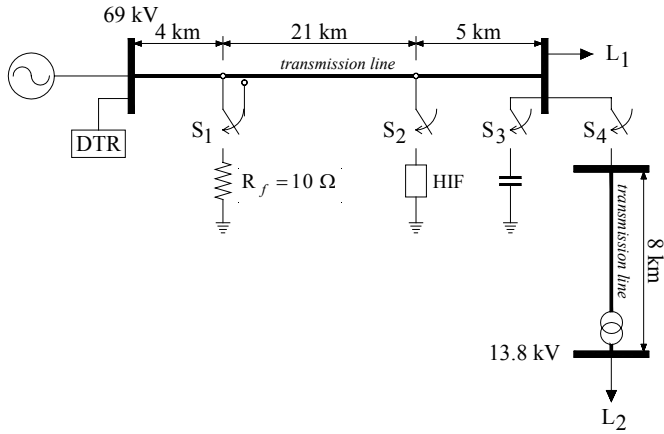


Fig. 6. Power system for case studies

A. Capacitor energization

In this case the capacitor bank was connected in parallel with a wye connection. The capacitors have 4 mS with a factor for the series resistance of 0.15. Figure 7a shows the part of v_d 's signal that contain the ignition of a transient due to the capacitor bank switch. The c_{diff}^2 signal and the adaptive threshold are depicted in Fig. 7b. It can be seen that the c_{diff}^2 is progressively larger than the adaptive threshold up to the third sample after the transient beginning. The fourth sample is below the threshold, but

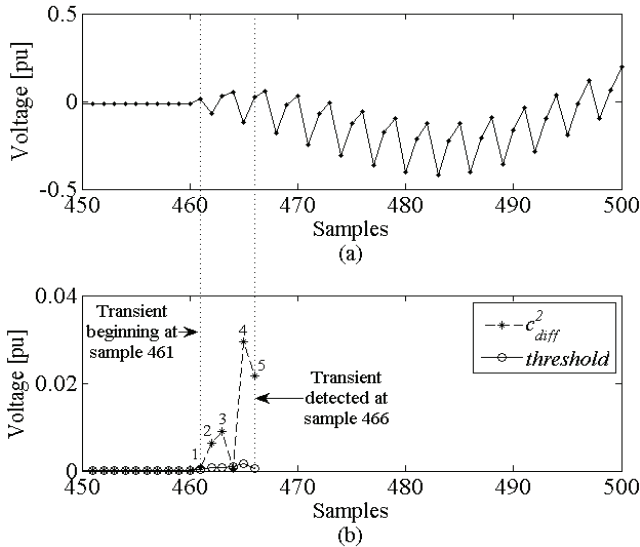


Fig. 7. Capacitor bank energizing detection: (a) v_d component; (b) adaptive threshold

fifth and sixth are above and confirm the transient detection. In this case the load had not produced an unbalance condition.

B. Transformer energization

In this case a 8 km long line was connected with a distribution transformer at the end of line with a balanced load. In Fig. 8 (b) is shown the value of count and it can be seen that the first value c_{diff}^2 after the transient beginning is much larger than the threshold. The second sample is below the threshold, but third is higher again. Subsequently oscillation due to the transient diminish and c_{diff}^2 become smaller, but always above the threshold, leading to transient confirmation at sample 466 of the v_d signal.

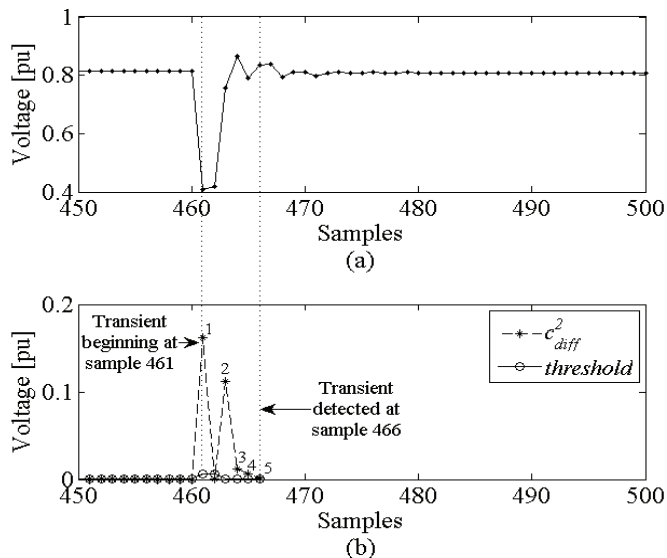


Fig. 8. Transformer energizing detection: (a) v_d component; (b) adaptive threshold

C. Permanent resistive fault

In Figure 9, the three-phase voltages from a permanent resistive fault in phase b at 4 km from the feeder can be seen. This confirms what was said in section one of the paper: a disturbance in one phase can produce disturbances in the others phases. As can be seen in Fig. 10 (b) oscillations due to travelling wave phenomenon are high at the beginning of the transient and first three samples of c_{diff}^2 are considerably above the threshold. The following samples are lower, but enough to confirm transient detection at sample 466 of v_d signal.

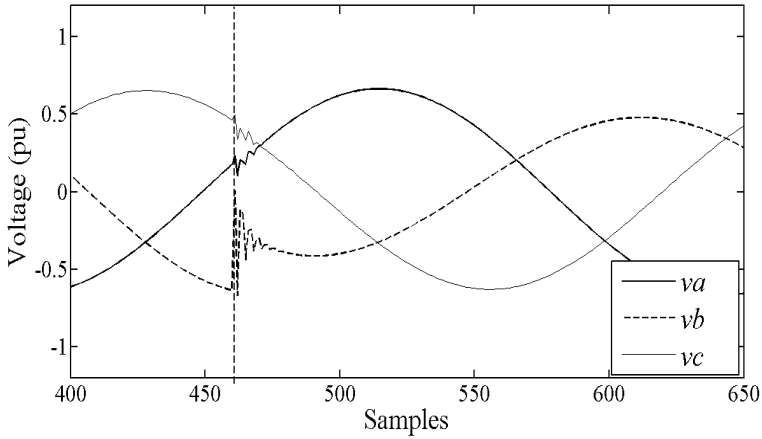


Fig. 9. Three phase voltage of single phase fault

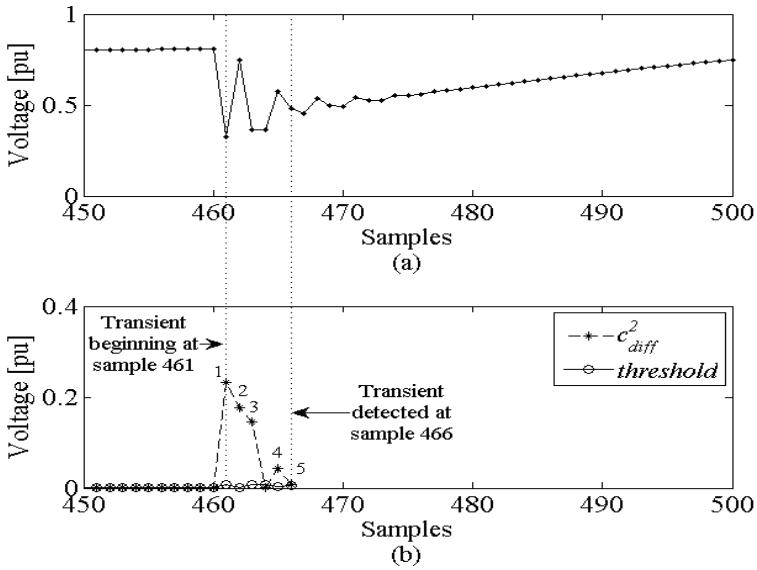


Fig. 10. Permanent resistive fault detection: (a) v_d component; (b) adaptive threshold

D. High impedance fault

A HIF modeled according to [4] was connected at 25 km from feeder in phase b . In this case transient was detected too with the proposed thresholds configuration. As can be seen in Fig. 12 (b), five samples after HIF inception are above the adaptive threshold, detecting the transient. As can be seen in Fig. 11 the voltage unbalance among phases is not significant, however can be seen an oscillation in v_d signal if it is calcu-

lated for more samples. As a HIF has some harmonic content, that oscillation can be explained by means of (23), replacing functions that represent transients by any harmonic component. This lead a function $m(t)$ with the same harmonic content but modified by the multiplication by a cosine with time varying phase.

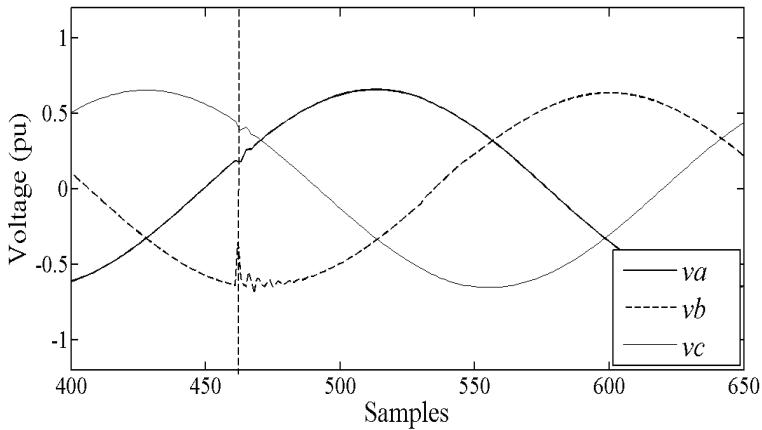


Fig. 11. Three phase voltage of single phase HIF

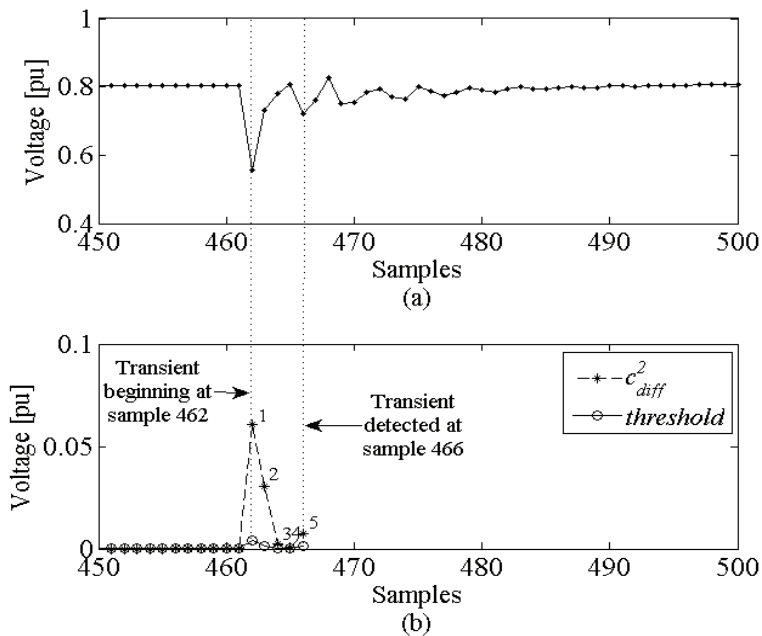


Fig. 12. HIF detection: (a) v_d component; (b) adaptive threshold

5. DISCUSSIONS

Application: In this paper, an analytical approach and a full algorithm for transient detection using the Park's transformation is presented. From the case studies shown, it is thus clear that Park's transformation is a useful and valid approach for transient detection in electrical power systems.

Advantages: Application of Park's transformation in three phase voltage signals brings some noticeable advantages. Firstly, all three phases can be monitored simultaneously by the analysis of only one signal. Secondly, when the system is operating normally (case *A* in section three), all Park's signals are constants, perturbed only in the presence of a transient (case *B* in section three). Naturally in practice it is not possible to have a perfectly equilibrated system free of noise, for this reason an adaptive threshold was presented. The algorithm has the possibility to control the sensibility of detection by means of an over-threshold samples-counter and a time-counter. Furthermore, this approach is insensitive to fault type, fault location, fault resistance, fault inception angle, switching operations or deviations in fundamental frequency of power system. Nonetheless, due to space, not all events have been presented in this work.

Limitations: The major limitation in the application of this approach is related to the frequency response of the voltage and current transformers. In fact, the transducers can introduce errors and attenuate the voltage and current signals.

Future Research: Classification and characterization of electromagnetic phenomena efficiently are classical problems in power quality engineering. Hence, future works can explore the application of Park's transformation in power quality applications. Also, the explicitly behavior of Park's components can be shown in cases of phase imbalance and the presence of harmonics. Furthermore, can also be explored the orthogonal behavior between v_d and v_q components for other applications.

6. CONCLUSIONS

A full analytical study on the Park's transformation has been presented within the context of transient detection analysis in electric power systems. In this paper it was presented a discussion of the application of Park's transformation for transient detection. The approach may use measurements of voltages or currents signals obtained in the local terminal from a power transmission or distribution systems.

The major contributions of this work are related to the presentation of the equations v_0 , v_d , and v_q components that show in detail the behavior of the three-phase signals in the presence of electromagnetic transients in all phases. The analysis of these equations was essential in order to understand the nature and response of its

solutions for some important operation conditions of the power system. Another important contribution is the presentation of a full algorithm for transient detection.

It is important to point out that this approach is insensitive to the event type and can be used for the detection of transient signals of the some typical operational situations in power systems. As demonstrated by the case studies, it is clear that Park's transformation introduces a further improvement for transient detection in power systems.

REFERENCES

- [1] Institute of Electrical and Electronics Engineers, *Recommended practice for monitoring electric power quality: Std. 1159*, IEEE Power Engineering Society, New York 1995.
- [2] SAHA M.M., IZYKOWSKI J., ROSOŁOWSKI E., *Fault Location on Power Network*, Springer-Verlag, New York 2010.
- [3] KIM C.J., RUSSEL B.D., *Harmonic Behaviour During Arcing Faults on Power Distribution Feeders*, Electric Power Systems Research, Vol. 14, 1988, 219–225.
- [4] EMANUEL A.E., GULACHENSKI E.M., *High Impedance Fault Arcing on Sandy Soil in 15 kV Distribution Feeders: Contribution to the evaluation of the low frequency spectrum*, IEEE Transactions on Power Delivery, Vol. 5, No. 2, 1990, 676–686.
- [5] WAI D.C.T., YIBIN X., *A Novel Technique for High Impedance Fault Identification*, IEEE Transactions on Power Delivery, Vol. 13, No. 3, 1998, 738–744.
- [6] MICHALIK M., REBIZANT W., ŁUKOWICZ M., LEE S., KANG S., *High-impedance fault detection in distribution networks with use of wavelet-based algorithm*, IEEE Transactions on Power Delivery, Vol. 21, No. 4, 2006, 1793–1802.
- [7] HE Z. FU L. LIN S. BO Z., *Fault Detection and Classification in EHV Transmission Line Based on Wavelet Singular Entropy*, IEEE Transactions on Power Delivery, Vol. 2, No. 4, 2010, 2156–2163.
- [8] MASOUM M.A.S., JAMALI S., GHAFFARZADEH N., *Detection and Classification of Power Quality Disturbances Using Discrete Wavelet Transform and Wavelet Networks*, IET Science, Measurement and Technology, Vol. 4, 2010, 193–205.
- [9] BAROS J., PÉREZ E., *Automatic Detection and Analysis of Voltage Events in Power Systems*, IEEE Transactions on Instrumentation and Measurement, Vol. 55, No. 5, 2006, 1487–1493.
- [10] LOPES F.V., SANTOS W.C., FERNANDES D., Jr., *An adaptive fault location method for smart distribution and transmissions grids*, IEEE PES Conference on Innovative Smart Grid Technologies (ISGT Latin America), Medellin, 19–21 Oct. 2011.
- [11] FERRAZ R.G., IURINIC L.U., FILOMENA A.D., BRETAS A.S., *Park's transformation analytical approach of transient signal analysis for power systems*, North American Power Symposium (NAPS), Urbana, 9–11 Sept. 2012.
- [12] KUNDUR P., *Power system stability and control*, McGraw-Hill, New York 1994, 83, eq. 3.118.
- [13] SPIEGEL M.R., *Mathematical handbook of formulas and tables*, McGraw-Hill, New York 1968, p. 15, eq. 5.35, p. 17, eqs. 5.66, 5.67.
- [14] BENMOUYAL G., MAHSEREDJIAN J., *A combined directional and faulted phase selector element based on incremental quantities*, IEEE Transactions on Power Delivery, Vol. 16, Iss. 4, 2001, 478–484.

Bartosz BRUSIŁOWICZ*
Janusz SZAFRAN*

INFLUENCE OF TRANSFORMER TAP CHANGER OPERATION ON VOLTAGE STABILITY

The paper concerns influence of transformer tap changer regulation on secondary voltage level and voltage stability margin of receiving node. At the beginning there are presented general information about voltage stability and tap changer. Voltage value of secondary terminals of transformer can be regulated using tap changer. This regulation also affects the calculation of Thevenin equivalent parameters seen from the secondary terminals. Changes of equivalent parameters cause a change of voltage stability conditions. Simulation studies of this influence for various types of load have been done. Selected simulation results are presented in the paper. At the end there are placed conclusions from the performed studies.

1. INTRODUCTION

Electricity delivered to customers should have appropriate quality. Required parameters are defined in European Standard EN 50160 [1]. One of the power quality parameters is the voltage value. The voltage variations can be caused by normal operation of power system – changes of power system configuration or parameters of loads. The power system can be designed to maintain the value of voltage in acceptable limits despite of these changes. However, randomly situations where these limits are exceeded can occur. To ensure constant voltage level, some of power system nodes should have a voltage control systems. This regulation, what is obvious, also affects other parameters of the operating point of power system node. The most commonly used methods of voltage adjustment are: voltage tap changer, reactive power compensation and undervoltage load shedding. This paper refers only to analysis of the influence of transformer tap changer operation on voltage level and voltage stability.

* Institute of Electrical Power Engineering, Wrocław University of Technology, Wrocław Poland.

Voltage stability is defined by IEEE in the following way: “Voltage stability is the ability of a system to maintain voltage so that when load admittance is increased load power will increase and so that both power and voltage are controllable” [2].

Margin of this stability can be determined using a full model of the power system and the power flow calculations. Voltage characteristics of loads can be added for such model. For each node stability margin can be calculated basing on changes of parameters caused by voltage variations e.g. $d\Delta Q/dV$ [3, 4].

To study voltage stability of selected power system receiving node, it is more convenient to use a simplified Thevenin equivalent model. In this model part of power system seen from the node may be replaced by ideal voltage source E and system impedance Z_S (Fig. 1).

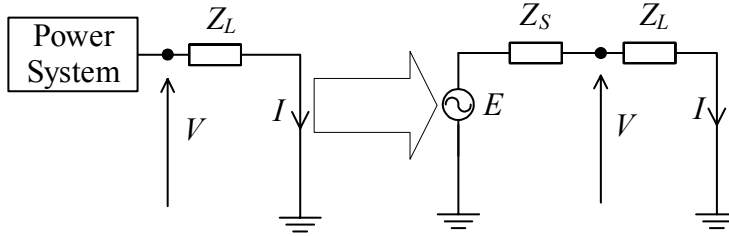


Fig. 1. Thevenin model

Parameters of stable operating point of presented Thevenin circuit are defined by the following equations [5]:

$$V = \frac{E}{\sqrt{1 + W^2 + 2W \cos \beta}}, \quad (1)$$

$$S = \frac{E^2 W}{Z_S (1 + W^2 + 2W \cos \beta)}. \quad (2)$$

where: V – node voltage, S – load apparent power, $W = Z_S/Z_L$, Z_S – system impedance, Z_L – load impedance, $\beta = \varphi_S - \varphi_L$, φ_S and φ_L – system and load phase angle.

Voltage stability limit occurs at the point of maximum power transfer [6]. In this point, the equation (3) is true. Thus, to calculate voltage stability margin it is more practical to use equation (4).

$$|\overline{Z_S}| = |\overline{Z_L}|, \quad (3)$$

$$\Delta W = 1 - W = 1 - \frac{|\overline{Z_S}|}{|\overline{Z_L}|}. \quad (4)$$

Value of load impedance is greater than system impedance, so W parameter is changing from 0 to 1. The power system receiving node is stable if value of W is lower than 1.

In the literature various methods of W parameter calculation can be found. These methods often use only locally available measurements of voltage and current. For example W parameter can be calculated using: equations of Thevenin model [6], derivatives of apparent load power against the node voltage dS/dV [7] or node voltage against load admittance dV/dY [8].

2. TRANSFORMER TAP CHANGER

To regulate the secondary voltage level separated coils of winding are connected to the tap changer at one of the transformer site, usually at the primary. Operation of the tap changer modifies the total number of active coils of primary winding. For a fixed number of coils at secondary winding, this action causes change of transformer voltage ratio.

Types of tap changers are divided into: De-Energized Tap Changer (DETC) and Load Tap Changer (LTC) [9]. DETC regulators are used in systems where need of voltage level changing occurs relatively rare. If the voltage value changes often LTC systems are used.

For Thevenin model (Fig. 1) voltage regulation using transformer tap changer can be added (Fig. 2a). In this model, the winding and core losses are omitted. Level of secondary voltage depends on the position of tap changer g according to equation (5)

$$g = \frac{V_L}{V_1} . \tag{5}$$

To eliminate the tap changer from presented model, Thevenin parameters to various windings of transformer can be calculated. The system impedance Z_S and voltage source E can be converted to the secondary winding according to the formula (6). Figure 2b shows Thevenin model with calculated parameters.

$$Z_S' = Z_S * g^2 \quad E' = E * g \tag{6}$$

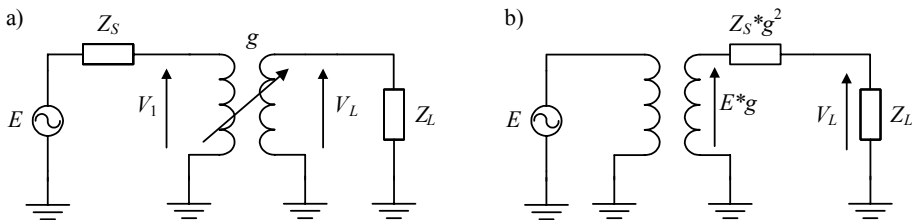


Fig. 2. Thevenin model with tap changer

Taking into account transformer ratio g in voltage equation (1), secondary voltage can be described by following formula:

$$V_L = \frac{Eg}{\sqrt{1 + (Wg^2)^2 + 2Wg^2 \cos \beta}}. \quad (7)$$

From equations (5) and (7) primary voltage can be calculated in the following way:

$$V_1 = \frac{V_L}{g} = \frac{E}{\sqrt{1 + (Wg^2)^2 + 2Wg^2 \cos \beta}}. \quad (8)$$

Above presented equations show that the change of tap changer position affects primary and secondary transformer voltage. When g parameter increases, secondary voltage raises and primary voltage decreases. Figure 3 shows an example of this relation. Curves have been plotted for following parameters: $E = 1$, $W = 0.3$, $\varphi_{ZS} = 85^\circ$, $\varphi_{ZL} = 15^\circ$. Derivatives of primary and secondary voltages against transformer ratio g and sum of these derivatives are shown in Figure 3b.

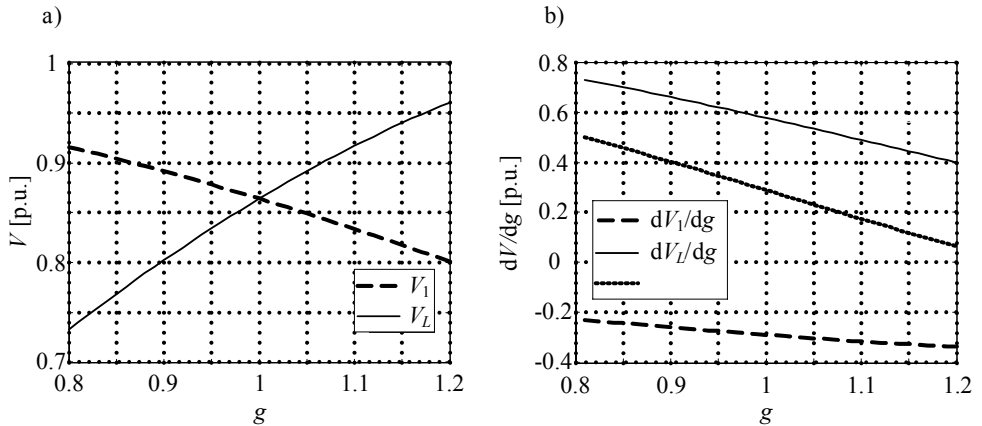


Fig. 3. Changes of primary and secondary voltage a) and derivatives b) for $W = 0.3$, $\beta = 70^\circ$

The derivative of the voltage against g ratio can be used as a criterion for tap changer operation blocking. The blocking should be performed when the changing tap changer does not provide desired effect. Such criterion has been described in literature [8]. The tap changer should be blocked when the derivatives of voltages are equal. Therefore, tap changer operation is allowed when the condition (9) is true. When this condition is not fulfilled, g ratio changing causes a greater decrease of primary voltage than increase of the secondary voltage. In such case, it is reasonable to block the tap changer.

$$\frac{dV_L}{dg} + \frac{dV_1}{dg} > 0 \tag{9}$$

3. SIMULATION RESULTS

Simulations of influence of tap changer operation on primary and secondary voltage changes have been performed. The following parameters of Thevenin model have been assumed: $E = 1$ $|Z_S| = 1$ $\varphi_{ZS} = 85^\circ$. Load angle φ_{ZL} , as in the previous case, has been 15° , so β angle has amounted 70° . Simulations have been performed for different values of the load impedance. The W parameter has taken following values: $W = 0,1; 0,3; 0,5$ and $0,7$. Figures 4–7 show changes of the primary and secondary voltage and derivatives of these changes.

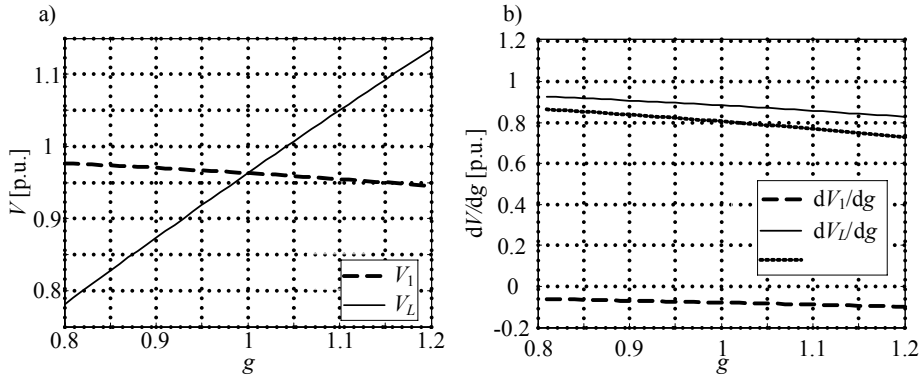


Fig. 4. Changes of primary and secondary voltage a) and derivatives b) for $W = 0,1, \beta = 70^\circ$

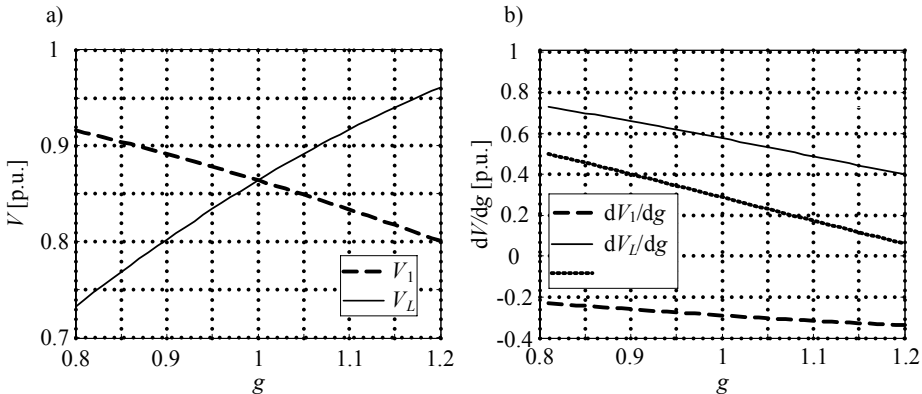


Fig. 5. Changes of primary and secondary voltage a) and derivatives b) for $W = 0,3, \beta = 70^\circ$

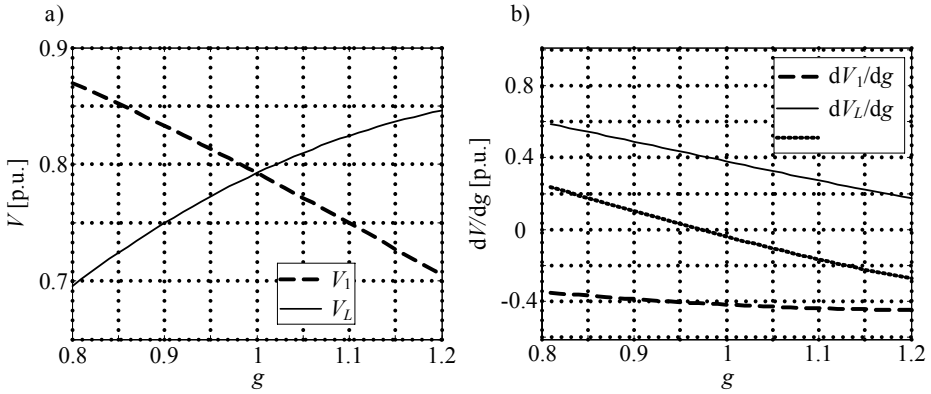


Fig. 6. Changes of primary and secondary voltage a) and derivatives b) for $W = 0.5$, $\beta = 70^\circ$

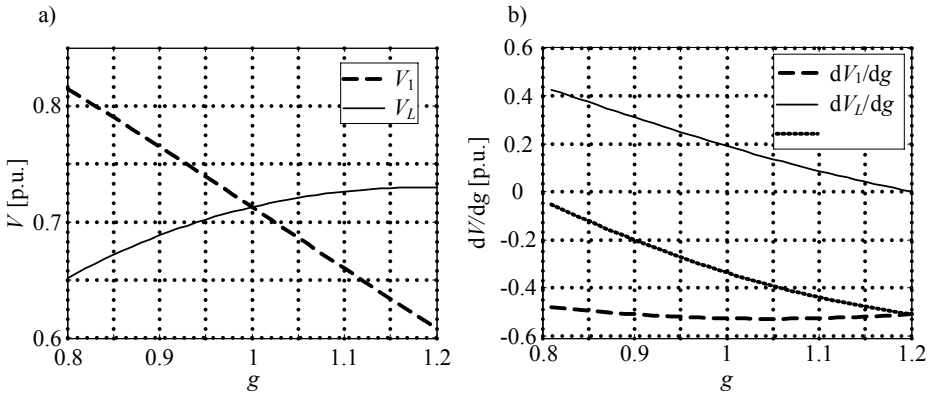


Fig. 7. Changes of primary and secondary voltage a) and derivatives b) for $W = 0.7$, $\beta = 70^\circ$

The presented plots show that the lean of curves depends on the W parameter. For small values of W (Fig. 4) regulation of secondary voltage V_L does not change significantly the primary voltage V_1 . Secondary voltage derivative dV_L/dg is positive and primary voltage derivative dV_1/dg is negative. In the operational range $g = 0.8:1.2$ sum of these derivatives will be greater than zero. So the condition (9) is true. Also, for $W = 0.3$ in the operational range sum of derivatives does not reach zero. Approaching to the end of range, the sum is close to zero. However, the tap changer should not be blocked. For $W = 0.5$ sum of voltages derivatives reaches zero for $g = 0.97$. When tap changer is in neutral position $g=1$ and such load occurs, any increase of the secondary voltage results in a large decreasing of primary voltage so the regulation is not effective. When $W = 0.7$ regulation of voltage is not effective over the operational range.

Different rates of changes of derivatives for various values of W parameter are caused by the increase of voltage and apparent power. Therefore, the operating point

is moved both upwards and in the direction of maximum power transfer. These contingencies for various values of W parameter are shown in Fig. 8. The solid line is the curve plotted for $g = 1$. Dashed lines indicate the transformer ratio changes to $g = 0.8$ and $g = 1.2$. Load characteristics are marked by dotted lines. Fig. 8 shows that for rising initial W parameter, increase rate of secondary voltage caused by tap changer operation is getting smaller and increase rate of apparent power is growing.

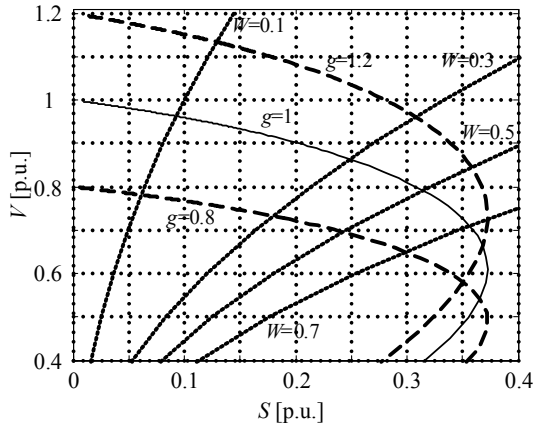


Fig. 8. Nose curves and load characteristics

It is obvious that changes of V_1 and V_L voltages also depend on the angle of the load impedance. For angles close to zero or negative (capacitive load) the initial voltage drop is smaller and regulation brings greater effect. Figure 9 shows sum of derivatives for $W = 0.4$ and three values of the load impedance angle. In the tap changer operational range blocking should be performed only for angle amounting $\varphi_{ZL} = 15^\circ$.

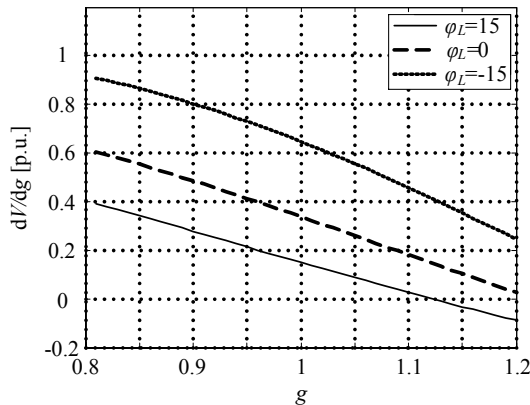


Fig. 9. Sum of derivatives for various load angles

Assuming that the limit of voltage stability occurs when $W = 1$ and that the change of tap changer position affects calculation of system impedance Z_S , equation (10) can be written. Equation (10) can be transformed to formula (11). This formula can be used to calculate limit tap changer position for which the circuit reaches the limit of stability. Changes of g_{lim} according to value of W variations are shown in Fig. 10.

$$W = W_1 * g^2 = 1, \quad (10)$$

$$g_{lim} = \frac{1}{\sqrt{W_1}}. \quad (11)$$

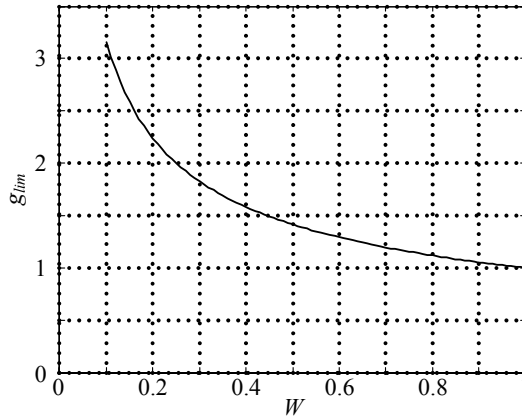


Fig. 10. Changes of g_{lim} according to W variations

It can be seen that the values of g_{lim} are greater than those resulting from quoted criterion based on measurement of voltage derivatives. In the presented example, for $W = 0.5$ blocking tap changer should be performed for $g = 1.125$ (Fig. 6). For this level of W parameter, value of $g_{lim} = 1.4$ (Fig. 10). This confirms the validity of voltages derivatives criterion. However, between the values of g resulting from this criterion and g_{lim} there is an area where the regulation might be performed.

4. NONLINEAR LOADS

Previous considerations have been carried out assuming that the load impedance is linear. However, in reality, the value of impedance depends on the voltage level. Example dependences are presented in the IEEE publication [9].

The simplest way of describing nonlinear load model is the exponential equation (12).

$$Z_L = Z_{L0} \left(\frac{V}{V_0} \right)^\alpha \quad (12)$$

where: Z_{L0} – rated impedance, α – exponent of voltage characteristic.

Examples of basic models (constant impedance, current and power) are shown in Fig. 11. The Figure shows that changes of voltage and apparent power are different for various load models. It can be concluded that the impact of tap changer regulation depends on α exponent (equation (12)).

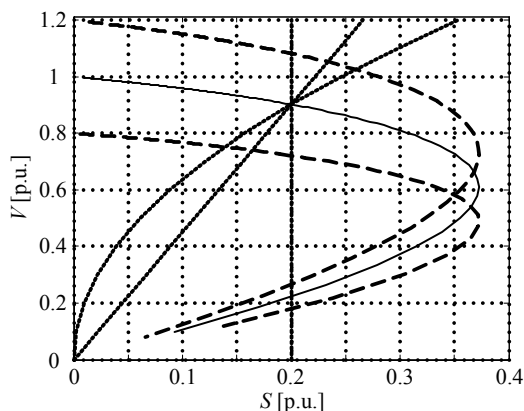


Fig. 11. Nose curves and load characteristics

For the fixed parameters of Thevenin model value of W depends only on the load impedance. In nonlinear model this impedance is changing according to value of secondary voltage. Converting the load impedance on the primary voltage and including dependence on voltage equation (13) can be obtained.

$$W_1 = \frac{Z_S}{Z_L} = \frac{Z_S}{Z_{L0} \frac{(V_1 g_1)^\alpha}{g_1^2}} \quad (13)$$

where: $V_1 = V_1/V_0$; V_0 – rated voltage.

The W parameter strongly depends on transformer ratio g . Equation 13 can be also written for changed value of g_2 . From both equations, system impedance Z_S can be determined. Comparing and transforming these two equations formula (14) can be calculated. W_2/W_1 parameter represents variations of W according to change of g and α exponent of load model.

$$\frac{W_2}{W_1} = \left(\frac{g_2}{g_1} \right)^{2-\alpha} \quad (14)$$

Changing the value of tap changer position g , curves corresponding to changes of W_2/W_1 parameter for fundamental load models have been plotted. These models have been: $\alpha = 0$ – constant impedance, $\alpha = 1$ – constant current, $\alpha = 2$ – constant power. Obtained curves are shown in Figure 12.

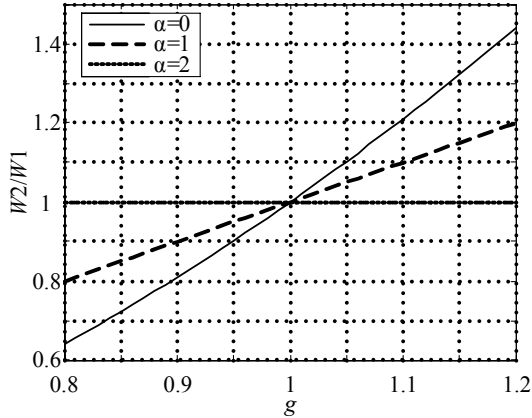


Fig. 12. Changes of W_2/W_1 parameter according to g variations

From Figure 12 it can be noticed that increase of W parameter is greater when α exponent is lower. The largest increase is for the constant impedance load and the lowest for constant power model. This contingency is similar to that shown in Figure 11. The greatest increase of load apparent power (getting closer to the stability limit) is for constant impedance model. If the load model is constant power, tap changer operation changes only value of voltage.

To transform load impedance to primary voltage, value of the impedance should be divided by squared transformer ratio g . Value of impedance of constant power model depends on squared secondary voltage. This voltage depends on g parameter. Therefore, W parameter is not changed.

Additional tests similar to those in section 3, using constant power model have been made. Formula (12) is nonlinear, so to perform simulations the method of solving nonlinear equations has been chosen. Aitken iterative algorithm has been used [10].

From Figure 13 it can be noticed that rising g parameter causes increase of secondary voltage level with no change of primary voltage. The derivative of primary voltage is zero and derivative of secondary voltage is positive. Therefore, the sum of derivatives will never reach zero. For constant power model, operation of tap changer can be carried out over entire range of regulation regardless of the W parameter and angle of the load.

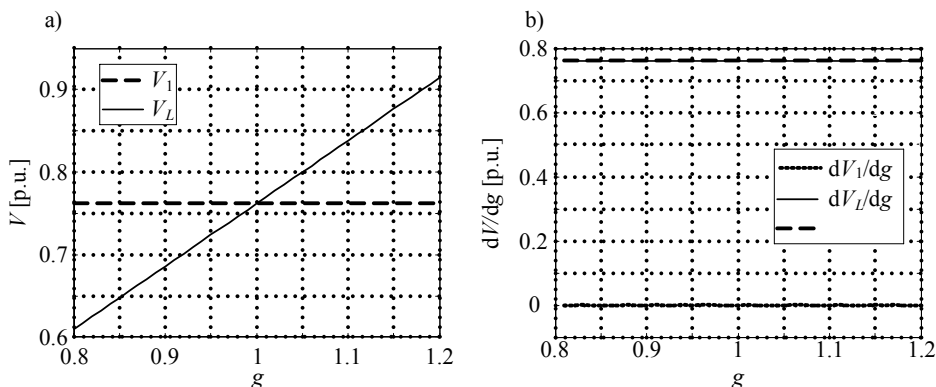


Fig. 13. Changes of primary and secondary voltage (a) and derivatives (b) for $W=0.3$, $\beta=70^\circ$ – constant power model

When voltage regulation using tap changer for constant impedance model is performed the voltage stability conditions are the worst. For this model the apparent power varies with the square of the transformer ratio g . Constant power model is the safest because the tap changer operation does not endanger safety of the node.

5. CONCLUSIONS

1. It is possible to block tap changer using quoted criterion when increasing secondary voltage level causes a significant decreasing of primary voltage. Blocking point is determined by measuring the derivatives of these voltages according to transformer ratio changes.

2. For each value of W parameter it is possible to calculate the critical transformer ratio. This value corresponds to transformer ratio which will result in loss of voltage stability. In the paper g_{lim} is calculated assuming linear load impedance. For other models, the critical value will be probably greater. Therefore, use of g_{lim} calculated for linear impedance to nonlinear models will result in greater safety margin obtained.

3. Value of g_{lim} parameter is greater than g level arising from the quoted criterion. Between them there is an area where the voltage regulation could be carried out maintaining given stability margin.

4. The effect of tap changer operation depends on load model. The paper describes the dependence of these effects according to value of α exponent.

5. When voltage regulation using tap changer is performed it is required to determine the impact of these actions on value of voltage and voltage stability margin.

REFERENCES

- [1] CENELEC, EN 50160:2010, *Voltage characteristics of electricity supplied by public electricity networks*.
- [2] BEGOVIC M., FULTON D., GONZALES M.R. et al., *Summary of System protection and voltage stability*, IEEE Transactions on Power Delivery, Vol. 10, Iss. 2, Apr. 1995, 637–638.
- [3] KREMENS Z., SOBIERAJSKI M., *Analiza systemów elektroenergetycznych*, WNT, Warszawa 1996, ISBN 83-204-2060-1 (in Polish).
- [4] MACHOWSKI J., BIALEK J.W., BUMBY J.R., *Power system dynamics: stability and control*, 2nd ed., John Wiley & Sons, Ltd., 2008, ISBN 978-0-470-72558-0.
- [5] WISZNIEWSKI A., *New Criteria of Voltage Stability Margin for the Purpose of Load Shedding*, IEEE Transactions on Power Delivery, Vol. 22, Iss. 3, July 2007, 1367–1371.
- [6] VU K., BEGOVIC M.M., NOVOSEL D., SAHA M.M., *Use of Local Measurements to Estimate Voltage Stability Margin*, IEEE Transactions on Power Systems, Vol. 14, No. 3, August 1999, 1029–1035.
- [7] BRUSIŁOWICZ B., REBIZANT W., SZAFRAN J., *A new method of voltage stability margin estimation based on local measurements*. APAP 2011 Conference, Beijing, No. 1790, 2443–2447.
- [8] WISZNIEWSKI A., REBIZANT W., KLIMEK A., *Intelligent Voltage Difference Control Maintaining the Voltage Stability Limit*. Proceedings of the 43th CIGRE Session, Paris, France, paper B5_107_2010, August 2010.
- [9] IEEE TASK FORCE ON LOAD REPRESENTATION FOR DYNAMIC PERFORMANCE, *Load representation for dynamic performance analysis*, IEEE Transactions on Power systems, Vol. 8, No. 2, May 1993.
- [10] ROSOŁOWSKI E., *Komputerowe metody analizy elektromagnetycznych stanów przejściowych*, Oficyna Wydawnicza PWr., Wrocław 2009 (in Polish).

Mateusz PUSTUŁKA*, Jan IŻYKOWSKI*,
Mirosław ŁUKOWICZ*

NEURAL NETWORK FILTRATION FOR ARC FAULTS LOCATION ON POWER TRANSMISSION LINES

This paper presents filtration using neural network for arc fault location, which allows to determine the distance to a fault, as a result of considering natural fault loops. It is assumed that three-phase voltages and currents from both ends of the line are the input signals of the fault locator and naturally of the neural network applied for filtering the input signals. In addition to natural fault loop signals also use of symmetrical components (positive and negative or incremental positive sequence components) to fault location were considered as well. Results of evaluation study have been included, analyzed and discussed. Influence of filtration has been also considered.

1. INTRODUCTION

The reliable operation of the electric power grid is one of the main goals of power system operators. Reduction of the duration of outages is one of the key requirements. There are many different ways that this goal can be achieved, with accurate fault location for an inspection-repair purpose [2, 5, 6] being one of them.

Algorithms for accurate location of faults on power lines have been a subject of great interest of researchers since the power system reliability became an important factor for network operators and customers [6]. Among the known methods, the approach based on an impedance principle is the most popular and most frequently implemented into protective relays or stand alone fault locators (FL). In particular, the algorithms utilizing one-end current and voltage measurements have been

* Institute of Electrical Power Engineering, Wrocław University of Technology, Wrocław, Poland.

introduced at the beginning. Then two-end fault location principle [5, 6] has been extensively explored. This principle is considered in this paper.

Neural networks are one of the fastest growing artificial intelligence techniques. Due to the ability to learn and adapt they have a high potential. Series of patterns based on heuristic knowledge are presented to neural network in the learning process. Artificial neural network acquires the ability to appropriately respond included in the learning database.

The main task for neural network applied in this study will be prediction of steady state signals obtained by using current and voltage signals from the interval just after fault inception. The computer models of transmission system developed for this purpose were used for generating large number of short-circuit cases. The variability ranges of the system parameters was adopted for modeling faults. Either fault location, fault resistance and short-circuit power of equivalent sources behind line terminals were changed in random. Size of population generated for neural network learning process was 1000 cases and for testing it was 100 cases. Results of evaluation study have been included and discussed.

Fault location algorithm was performed using the signals generated by simulating arc faults on the transmission line: 400 kV (Fig. 1), 50 km with the aid of ATP-EMTP software [1]. The representative results for the single-phase arc fault: L1-E are presented further. Current and voltage measurements were carried out at both ends of the line.

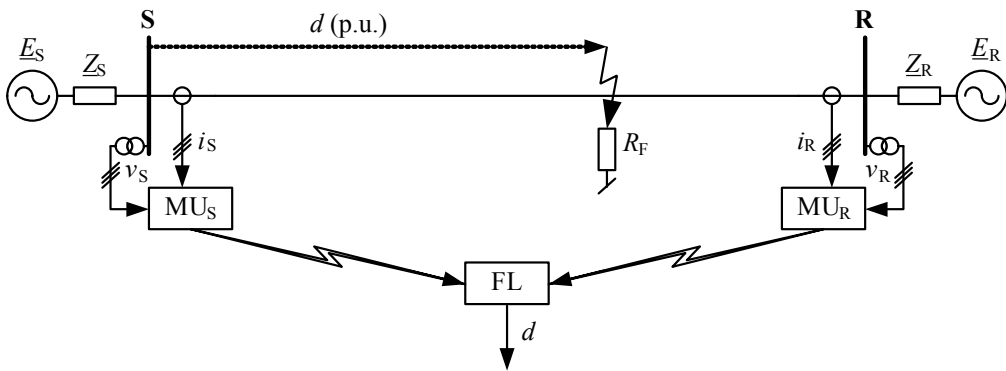


Fig. 1. Schematic diagram of two-end fault location

2. ARC FAULTS

The main aim of this study is to develop a neural network filtration for arc fault locator, therefore suitable arc fault model had to be introduced to the system model. Dynamic arc model was adopted in the form of the differential equation [3]

$$\frac{dg_p}{dt} = \frac{1}{T_p} (G_p - g_p) \tag{1}$$

where:

- g_p – dynamic arc conductance,
- G_p – stationary arc conductance,
- T_p – time constant.

Using the ATP-EMTP program [1] for arc fault simulation, the arc can be reflected with the non-linear resistor – defined in the ELECTRICAL NETWORK unit, while the arc model – in the MODELS (Fig. 2). The arc current (Fig. 3a, b) as the input quantity is measured on-line and the non-linear differential equation (1) is being

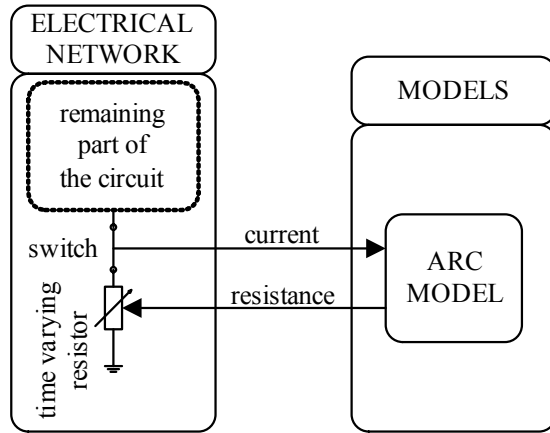
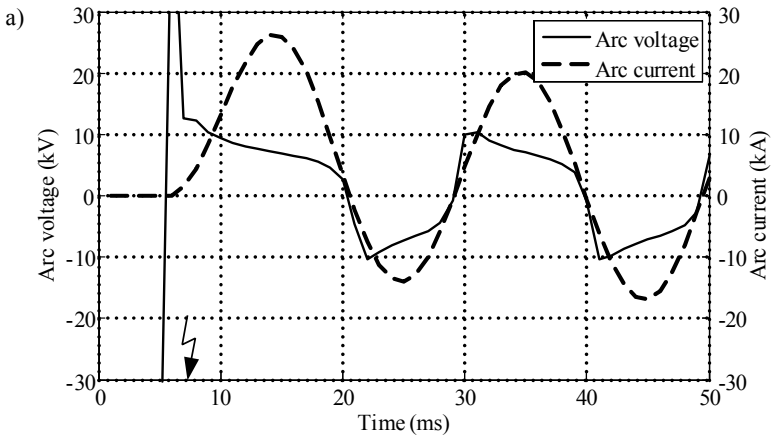


Fig. 2. Modeling arc with ATP-EMTP



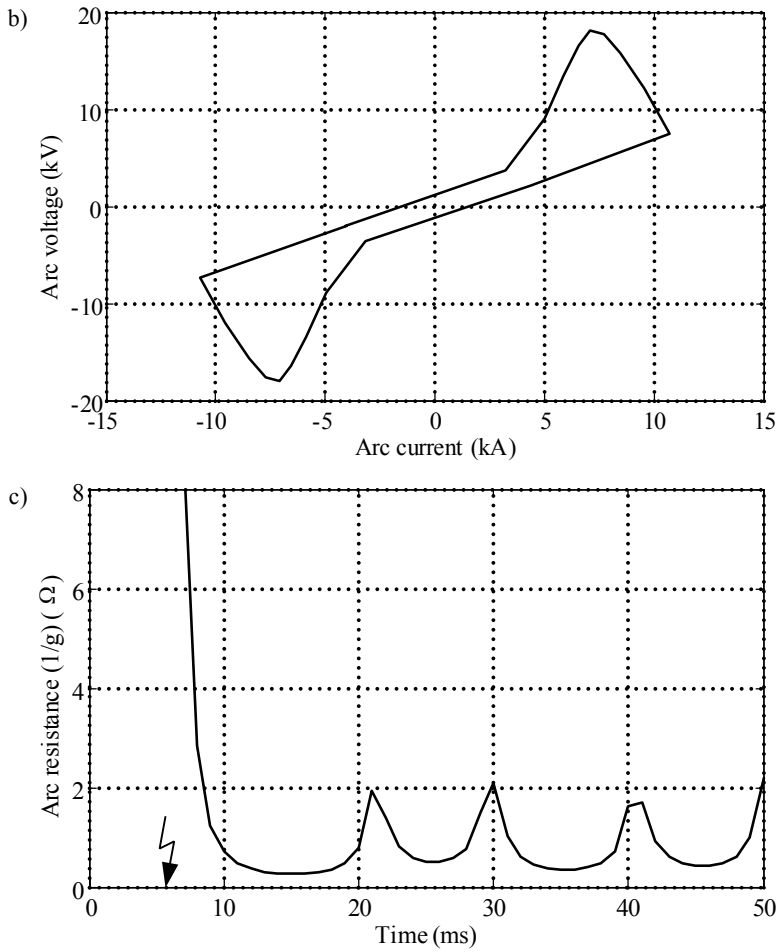


Fig. 3. Modeling of arc: a) arc current and voltage, b) arc voltage vs. arc current (for single cycle), c) arc resistance

solved. As a result, the arc resistance is determined and transferred for fixing the resistor modeling the arc.

The model (1) allows the arc conductance $g(t)$ to be determined, from which the arc resistance is calculated (Fig. 3c).

3. FAULT LOCATION ALGORITHM

Natural fault loops, identical as for a distance protection, are considered [4, 5]. For this purpose, the relaying signals (both voltage and current fault loop signals) are

formed accordingly to the fault type. Table 1 defines those signals to any consideration of fault loops seen from the S end of the line for a single-circuit line (Fig. 4). Signals for fault loop seen from the R end are composed analogously.

In a case of phase-to-earth fault the voltage and current of a given faulted phase are taken, but the component associated with the zero-sequence component: zero-sequence current (\underline{I}_{S0}) multiplied by the factor: $k_0 = (\underline{Z}_{0L} - \underline{Z}_{1L})/\underline{Z}_{1L}$ is added to the phase current. This results from the fact that the impedances of the line for the positive sequence (\underline{Z}_{1L}) and zero sequence (\underline{Z}_{0L}) are not identical, and the impedance of the line section between the measuring point (S) and the fault point (F) for the positive sequence ($d\underline{Z}_{1L}$) is a measure of the distance to fault (d (p.u.)) – Fig. 4.

For a fault loop phase 1-to-phase 2, the differences of voltages and currents from the phases involved in the fault, respectively, are taken as the fault loop signals. As a result of the subtraction, the zero sequence component is eliminated and there is no compensation due to different line impedances for the positive and zero sequences.

Figure 4 shows the models of the considered fault loops (Fig. 4a, b) and the aggregated model (Fig. 4c).

Table 1. Composition of fault loop voltage and current signals for single-circuit line

Fault type	Fault loop voltage	Fault loop current
L1-E	\underline{V}_{S_L1}	$\underline{I}_{S_L1} + k_0 \underline{I}_{S0}$
L2-E	\underline{V}_{S_L2}	$\underline{I}_{S_L2} + k_0 \underline{I}_{S0}$
L3-E	\underline{V}_{S_L3}	$\underline{I}_{S_L3} + k_0 \underline{I}_{S0}$
L1-L2, L1-L2-E, (L1-L2-L3, L1-L2-L3-E)*	$\underline{V}_{S_L1} - \underline{V}_{S_L2}$	$\underline{I}_{S_L1} - \underline{I}_{S_L2}$
L2-L3, L2-L3-E	$\underline{V}_{S_L2} - \underline{V}_{S_L3}$	$\underline{I}_{S_L2} - \underline{I}_{S_L3}$
L3-L1, L3-L1-E	$\underline{V}_{S_L3} - \underline{V}_{S_L1}$	$\underline{I}_{S_L3} - \underline{I}_{S_L1}$
* – includes loop L1-L2, but also loops L2-L3, L3-L1 can be analyzed, $k_0 = \frac{\underline{Z}_{0L} - \underline{Z}_{1L}}{\underline{Z}_{1L}}$.		

Fault loop seen from the S end (Fig. 4a) consists of a line section of the positive sequence impedance: $d\underline{Z}_{1L}$ and the transverse branch that represents a fault (resistance: R_{arc}). In case of the fault loop seen from the R end (Fig. 4b) impedance of the line section for the positive sequence is: $(1 - d)\underline{Z}_{1L}$ and the transverse branch is as in the previous fault loop (Fig. 4a).

Comparison of voltage on the transverse branch, i.e. at the fault point (F) – determined from the S and R line ends (Fig. 4), respectively, yields:

$$\underline{V}_{Sp} e^{j\delta} - d \underline{Z}_{1L} \underline{I}_{Sp} e^{j\delta} = \underline{V}_{Rp} - (1-d) \underline{Z}_{1L} \underline{I}_{Rp} \quad (2)$$

Equation (2) can be written separately for the real and imaginary parts. This gives a system of two equations with two unknowns: d – fault distance (p.u.), δ – synchronization angle. It can be solved using very well-known numerical procedures. However, one may face problems with obtaining a valid solution. In fact, the unknowns are: d , $\sin(\delta)$, $\cos(\delta)$ while the synchronization angle δ can be positive or negative, i.e. in the following range: $-\pi \leq \delta \leq \pi$. Only one solution, out of two, is a valid one.

In order to avoid iterative calculations it is proposed to specify the modulus (absolute value) for the synchronization operator $e^{j\delta}$ determined from (2) as follow:

$$|e^{j\delta}| = \left| \frac{\underline{V}_{Rp} - \underline{Z}_{1L} \underline{I}_{Rp} + d \underline{Z}_{1L} \underline{I}_{Rp}}{\underline{V}_{Sp} - d \underline{Z}_{1L} \underline{I}_{Sp}} \right| \quad (3)$$

This gives:

$$|\underline{V}_{Rp} - \underline{Z}_{1L} \underline{I}_{Rp} + d \underline{Z}_{1L} \underline{I}_{Rp}| = |\underline{V}_{Sp} - d \underline{Z}_{1L} \underline{I}_{Sp}| \quad (4)$$

After tedious manipulations on (4) the following quadratic equation for the sought distance to fault is obtained:

$$A_2 d^2 + A_1 d + A_0 = 0 \quad (5)$$

where: A_2 , A_1 , A_0 – coefficients (real numbers) specified by the phasors of fault loop signals [4]: $(\underline{V}_{Sp}, \underline{I}_{Sp})$ and $(\underline{V}_{Rp}, \underline{I}_{Rp})$, obtained with unsynchronized measurements at both ends of the line, and by the impedance of the line for the positive sequence (\underline{Z}_{1L}).

The solution of (5) gives two results for the sought fault distance (d_1, d_2). At least one of them indicates a detected fault in the line. If only one solution is such that it is satisfied: $0 < (d_1 \text{ or } d_2) < 1$, then in a natural way this solution is taken as the correct (valid). On the other hand, if it is obtained that the two solutions indicate a fault in the line: $0 < (d_1 \text{ and } d_2) < 1$, an additional selection of a solution that is correct has to be performed. Determination of the correct solution, which corresponds to the actual fault, can be determined by analyzing the estimated fault location when the input signals of the fault locator are symmetrical components of voltages and currents from both ends of the lines (Fig. 5).

As the input signals of the fault locator also symmetrical components of voltages and currents from both ends of the lines can be used: positive and negative – for asymmetrical faults, positive and incremental positive – for symmetrical three-phase faults.

In this case one needs replacing the fault loop signals in the derived equations (5) by the corresponding symmetrical components.

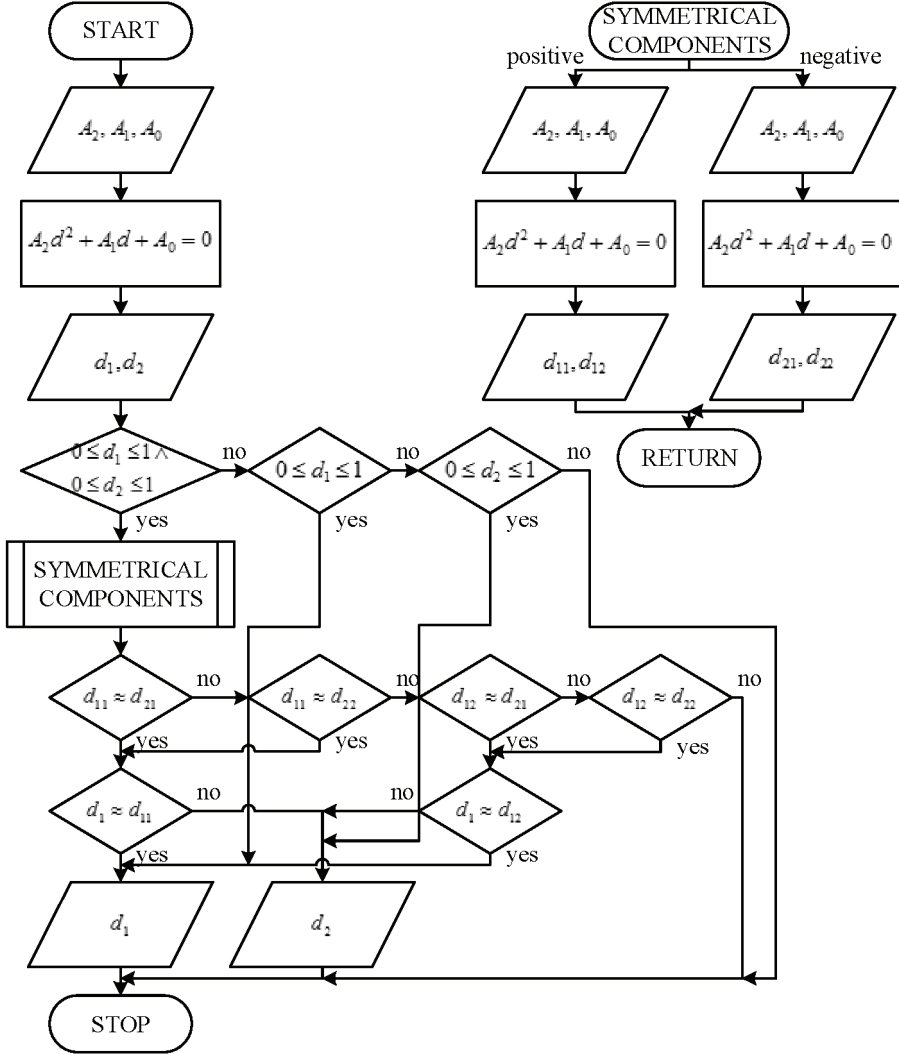


Fig. 5. The flowchart for calculating valid solution (main program with sub procedure)

4. ARTIFICIAL NEURAL NETWORK

Artificial neural network (ANN) used in the study contains two hidden layers consisting of 20 neurons and the output layer with 1 neuron (Fig. 6). Input vectors were

selected from the period 20ms just after fault (Fig. 7). A block diagram (Fig. 8) presents position of ANN in location procedure. There are used as many neural networks as many signals have to be filtrated.

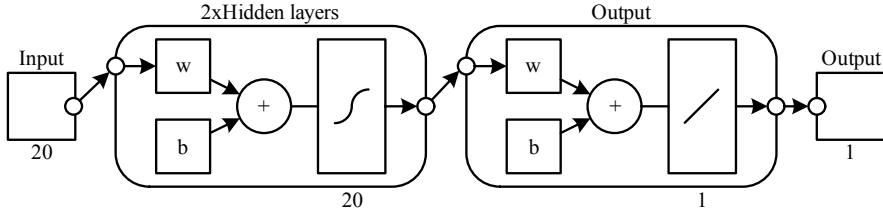


Fig. 6. Multilayer ANN

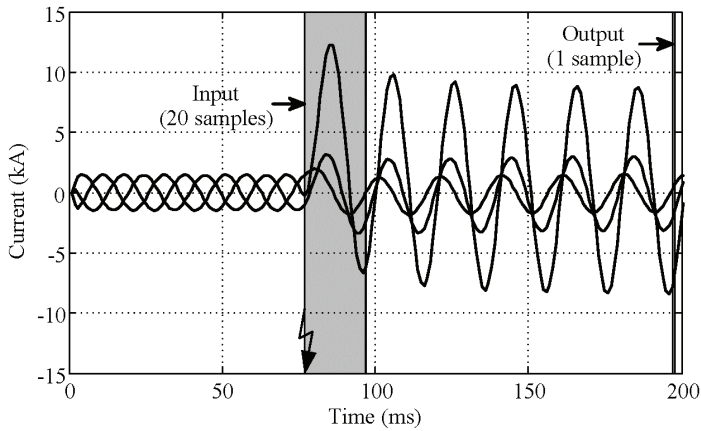


Fig. 7. Example of input and output of i_s for training ANN

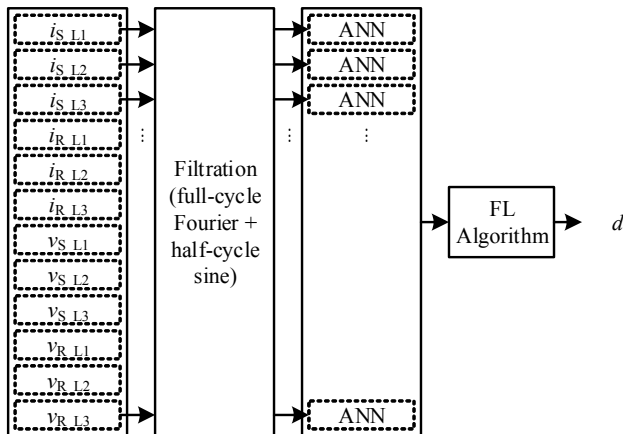


Fig. 8. The flowchart of investigated method

Before starting the learning process, inputs and outputs of the network were normalized using the scaling function so that it always belonged to the range $(-1, 1)$ and divided into learning, testing and validation data, respectively in a ratio of 70–15–15 cases. Network output corresponds directly to the target values. Tests were performed on different data (size of the population approximately 100 cases).

5. RESULTS

In statistical evaluation of the accuracy of particular fault location method, different measures for the fault location error are determined, as maximum, average, median (which gives result more resistant to extreme values, outlier elements) and standard deviation values. It is characteristic that the absolute value is usually taken for the nominator from the definition of the fault location error formula, thus can be written as follow

$$\text{Error}(\%) = \frac{|d - d_{\text{exact}}|}{l} 100\% \quad (6)$$

where:

d, d_{exact} – estimated and exact distance to the fault (in km or in relative units: p.u.),
 l – total line length (in km or in if relative units are used: $l = 1$ p.u.).

Table 3 presents solutions taken in 20ms after fault incipience for arc fault location algorithm and for arc fault location algorithm when solutions have been taken in 40ms after fault incipience. Both cases were considered with and without ANN.

Standard full-cycle Fourier filtration was used as the basic in the considered location algorithms. It has been found that in some cases, the applied such filtering alone appears as insufficient due to a severe distortion of the processed signals. It was a subject of research that performing the averaging of the results of the location in the fourth cycle after the fault, instead of averaging in the third cycle, significantly improves accuracy. Of course, this is possible only if the fault is not switched off earlier. An alternative approach to this is based on introducing an additional pre-filtering, leaving the averaging within the 3rd cycle – as was assumed at the beginning of the study. Additional pre-filtration was used with a half-cycle sine filter. It has been found that such extra pre-filtering contributes to a significant improvement of the fault location accuracy.

Selection of the valid solution (consistent with the actual fault) out of the two obtained from the quadratic equation (5) was performed as follows: the valid solution is determined by taking the solution for which there is a coincidence of the results obtained for two different components (when the input signals of the fault locator are symmetrical components of voltages and currents from both ends of the

lines), which in practice means that they are very close to each other, while for the other solution (to be rejected) there are significant differences; only one of the solutions for the fault distance indicates a fault in the line and it is naturally assumed to be the valid solution.

Table 3. Results for 10 from 100 test cases

Accurate fault distance (km)	ANN + Algorithm_t ₂₀ (km)	Error [%]	Algorithm_t ₂₀ (km)	Error [%]	Algorithm_t ₄₀ (km)	Error [%]	ANN + Algorithm_t ₄₀ (km)	Error [%]
5,00	5,11	0,22	5,14	0,28	5,06	0,13	4,93	0,14
10,00	10,32	0,64	7,57	4,86	10,10	0,20	9,99	0,03
15,00	14,84	0,31	12,49	5,03	15,33	0,65	14,82	0,36
20,00	20,54	1,09	21,14	2,28	19,72	0,56	19,98	0,04
25,00	25,02	0,05	30,00	10,00	24,57	0,86	24,87	0,27
30,00	30,45	0,89	29,05	1,89	29,93	0,15	29,82	0,36
35,00	35,19	0,37	36,70	3,40	34,91	0,19	33,06	3,88
40,00	39,17	1,67	37,47	5,06	39,78	0,43	39,57	0,87
45,00	44,86	0,29	54,86	19,71	43,91	2,18	44,93	0,14
max		1,67		19,71		2,18		3,88
average		0,61		5,83		0,59		0,68
median		0,37		4,86		0,43		0,27
std. deviation		0,52		5,89		0,65		1,23

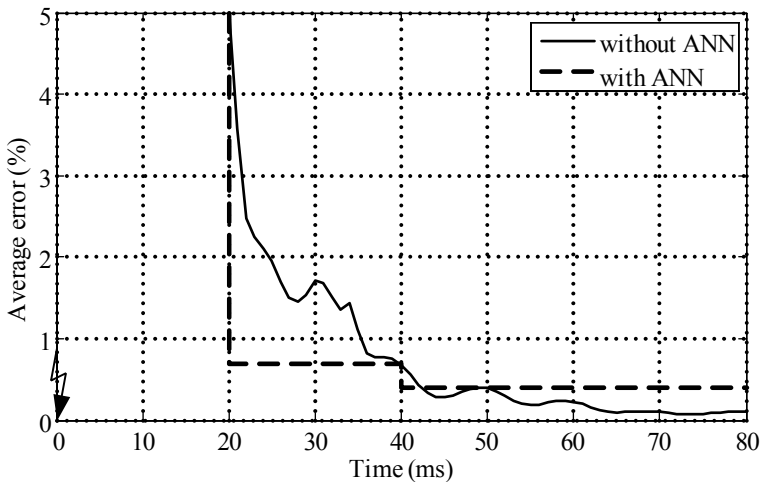


Fig. 9. Comparison of average error for algorithm with and without ANN

Better accuracy was achieved by using fault loop signals and it is slightly better than the location with using of the measured data from one end of the line. This is the effect that in case of measurements at one end only, as a result of insufficient information there is a need for introducing simplifying assumptions.

Comparison of fault location methods (with and without ANN) is shown in Fig. 9. In both cases there has been used the standard full-cycle Fourier filtering combined with the pre-filtering in the form of a half-cycle sine filter.

6. CONCLUSION

Arc fault location on transmission lines with use of voltage and current measurements from both ends of the line acquired asynchronously has been considered. The derived algorithm applies the fault loop signals from the two ends of the line as the fault locator inputs. Quadratic equation for the sought distance to fault, whose coefficients are expressed in a compact form, has been obtained. The selection of the valid solution (out of the two possible) is obtained by taking the solution for which there is a coincidence of the results obtained for two different components (when the input signals of the fault locator are symmetrical components of voltages and currents from both ends of the lines).

The derived algorithm can also be useful when symmetrical components of measured voltages and currents are applied as the only locator input signals. One should then use: positive and negative sequence components for asymmetrical faults and positive and incremental positive sequence for three-phase symmetrical faults. For a valid solution there is a coincidence of the results obtained for two different components, which in practice means that they are very close to each other, while for the other solution (to be rejected) there are significant differences. This approach was used as an assistance for calculating the valid solution.

The results of the study indicate the important role of digital filtering of the processed signals that are severely distorted under arc faults. It is reasonable to take a direct result of the calculations or results averaged – as late as possible after fault incipience, but before its elimination. It has been shown that using the standard full-cycle Fourier filtering combined with the pre-filtering in the form of a half-cycle sine filter and additional ANN improves considerably the accuracy of the calculation results. Moreover the results with lower errors are estimated in shorter time.

Analyzed application of measurements from both sides of the line to fault location does not require introducing the simplifying assumptions, which are necessary if the location is performed with only the local measurements. As a result, better accuracy is obtained. Further improvement of fault location accuracy can be achieved by taking into account the distributed-parameter line model for lines of considerable length.

Fault location algorithm with neural network filtration compared with alone algorithm gives better results. A comparative analysis has been prepared based on average error, median, maximum and standard deviation. Presented average errors of convergence show neural network as a method characterized by lower errors than algorithm which gives solution after 20ms and comparable results than algorithm with solution after 40ms.

REFERENCES

- [1] DOMMEL H.W., *Electro-Magnetic Transients Program*, BPA, Portland, Oregon, 1986.
- [2] FILOMENA A.D., RESENDER M., SALIM R.H., BRETAS A.S., *Fault location for underground distribution feeders: An extended impedance-based formulation with capacitive current compensation*, International Journal of Electrical Power & Energy Systems, Vol. 31, No. 9, October 2009, 489–496.
- [3] JOHNS A.T., AGGARWAL R.K., SONG Y.H., *Improved techniques for modelling fault arcs on faulted EHV transmission systems*, Generation, Transmission and Distribution, IEE Proceedings, Vol. 141, No. 2, 1994, 148–154.
- [4] PUSTUŁKA M., IŻYKOWSKI J., ŁUKOWICZ M., *Zastosowanie sztucznych sieci neuronowych do lokalizacji zwarć łukowych na elektroenergetycznych liniach przesyłowych*. Sieci Elektroenergetyczne w Przemśle i Energetyce, VII Konferencja naukowo-techniczna, Szklarska Poręba, 19–21 września 2012.
- [5] SAHA M.M., IŻYKOWSKI J., ROSOŁOWSKI E., *Fault Location on Power Networks*, Springer, London 2010.
- [6] SAHA M.M., ROSOŁOWSKI E., IŻYKOWSKI J., *New fault location method – incorporated in current differential protective relays for series compensated transmission lines*, PACWorld, Vol. 21, September 2012, 54–59.

Piotr SAWKO*, Kevin HILL*,
George EVANS*

DESIGN AND TESTING OF POWER SYSTEM PROTECTION FUNCTIONS USING SIMULINK[®] AND EMTP

This paper presents how simulation of power system behaviour under different disturbances can be used to test protection algorithms. A method for co-simulation using Electromagnetic Transient Program (EMTP) and Simulink is presented along with the procedure used for testing protection algorithms against different power system waveforms. The advantages of model based design are described showing how a realistic model of protection relay can be designed and how individual components are integrated.

1. INTRODUCTION

Modern numerical protection relays are used in many different applications. It is therefore of paramount importance to verify that each of the protection functions will operate exactly as expected, even during unusual disturbances. Early detection of any problems is also beneficial as it removes the necessity of rework allowing for a shorter time to market. With advancement in computer aided design (CAD) software and wide availability of high performance computers it is possible to test power system protection functions more comprehensively than ever before. First a short description of both tools is given as well as justification for using them. Then, the principles of model based design are discussed showing what benefit it can bring for the protection designer. In the following sections the details of co-simulation between EMTP and Simulink are described. The paper concludes with test results of a simplified under frequency function as an example of the capabilities of the method. An example is shown of function design in Simulink and power system model in EMTP.

* Schneider Electric UK, Ltd.

2. SIMULATION TOOLS

2.1. SIMULINK

Simulink is a graphical design tool allowing modelling of both continuous and discrete systems. It contains a wide range of blocks suitable for modelling control and signal processing algorithms allowing the designer to use his domain knowledge and not requiring him to become a software expert. Simulink allows the user to create his own reusable libraries which promotes the idea of component reuse and encapsulation as each of the libraries are self contained. Because of the graphical interface it is much easier to explain the concept to others while still being able to demonstrate how the model behaves under different application scenarios.

Simulink was chosen as a design tool because of the already mentioned simplicity of use as well as very good integration with Matlab which facilitates scripting. This is extremely important if it is planned to automate some of the testing done on the models.

2.2. EMTP-ATP DRAW

EMTP-ATP Draw is a power system simulation tool with a graphical user interface. It contains library blocks, allowing the simulation of behaviour of different power system equipment. With the library being constantly updated, this is one of the most popular software programs for power system simulations and is widely used in both academic and industrial applications. Because of the large number of ready to use components it is easy to create a model with the right level of detail, giving a compromise between accurate results, speed of simulation and the time necessary to produce the model.

This tool has been chosen since it is widely recognized for its accurate results as well as its fast solver allowing the tests to be run in shorter time compared to other simulation programs.

3. MODEL BASED DESIGN

With the computational power of modern computers it is possible to perform extensive testing of the designed functionality without having to produce costly prototypes. Model based design (MBD) facilitates early testing of algorithms, therefore making it easier to debug them and test against different scenarios. In the early stages of development only the general requirements are known therefore the model is relatively simple and many assumptions are initially made. As the work on the model progresses it becomes closer to the final product. The confidence in the de-

signed solution increases as more tests are conducted on the model. This can range from recording the response of the function to ideal signals (during initial stages of design) to responses to actual waveforms that can exist on the power system. After the algorithm is thoroughly tested it can then be implemented to run in the final product. This way most errors are found early in the design and little rework is required after the algorithm is implemented in the relay. The workflow of MBD is shown in Fig. 1.

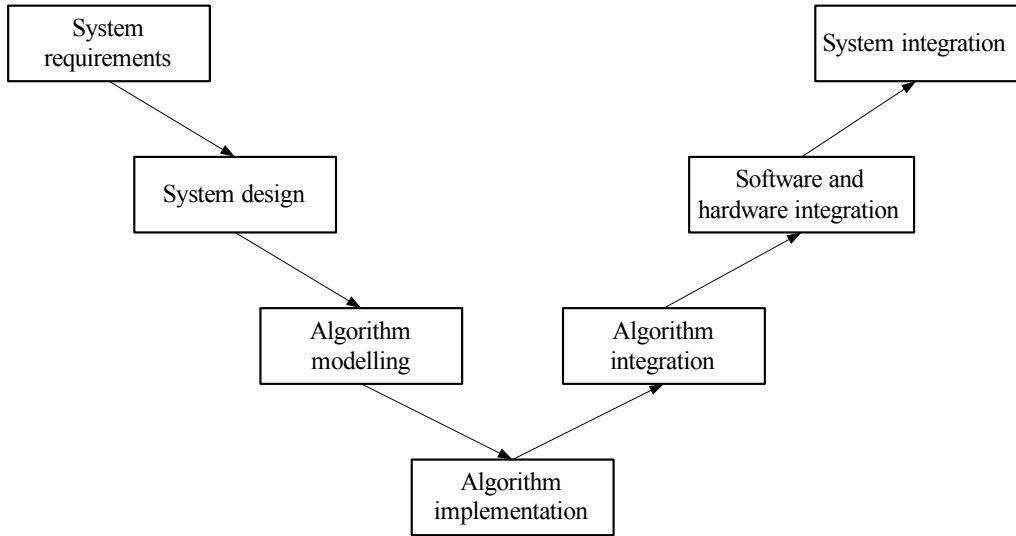


Fig. 1. Workflow in model based design development

With the initial design only the core algorithm is tested and the impact of the rest of the system is ignored. Many protection functions operate on the magnitude of a waveform and therefore in an early stage of development the testing is done using constant signals as opposed to sine waves. This simplifying assumption can be a source of many errors which will be detected in the later stages of development.

With the design tested using constant signals one can remove some of the assumptions by modelling the signal processing that will be used in the final product. This way it will be possible to confirm whether the algorithm still operates correctly even if the input signal is distorted by the signal processing. At this stage performance of the final product can be estimated with two main sources of delay being modelled. With signal processing being modelled it is possible to use both ideal sine waves as well as real power system waveforms as test vectors. This way the new algorithm can be tested using waveforms which are known to have caused problems for existing algorithms.

Since modern digital relays have advanced disturbance recording capabilities it is common to use those waveforms when testing new product or protection functions.

The level of detail of the model can be increased by modelling other parts of the final product like current transformers, anti aliasing filters, analog to digital converters, tripping contacts, etc. The more detailed the final model is the more confidence one has that performance of the model will be the same as the performance of the final product. If any problems are discovered during the design they can be addressed early on.

The important thing is that all the tests are stored, so if in the future a change in the algorithm is required regression testing can be easily done. Simulation of the algorithm used in the final product is also an easy way of error finding in case of relay mal operation.

MBD can make the design process much easier through the use of common library blocks which can be shared between designers and products. In this way common blocks of functionality have to be designed and tested only once. This reduces the risk of introducing errors in the algorithm as well as accelerating the design stage. An example of a common block can be a specific type of timer or a filter.

Simulink supports common block libraries and allows traceability between the instance of the block and the master copy of the library. In this way changes done to the library are automatically cascaded throughout the design. During initial testing sometimes it may be required to do some changes to the instance itself – this is possible by temporarily disabling the link. This allows the instance to be modified however it is still possible to restore the instance with the functionality in the library.

This paper describes how MBD can be implemented using Simulink however most of the techniques described can be realized using other tools as well.

4. CO-SIMULATION BETWEEN SIMULINK AND EMTP

The design process described in the previous section assumes that real power system waveforms are available for testing of the protection functions. This however is not always the case. Some fault scenarios are much more common than others so then it is possible that a real waveform can be used for testing. There are however many scenarios which are rare and no real waveforms are available.

This problem can be addressed by using modelling tools in order to understand the behaviour of the system during different types of disturbances.

The advantage of this approach is that many test waveforms can be generated to simulate scenarios relevant to the protection function under test. One example can be the testing of a distance relay by applying faults at specific locations on the line with different values of fault resistance. Such a comprehensive test would be almost impossible to do if one wanted to use only waveforms recorded on the power system, as this would require the fault to appear at exactly the same location but with different fault resistance each time. This however can be easily achieved by using power system simulation software.

With the increased number of tests running them all and analysing the results one by one can be a very slow process. If one continues with the distance protection example – for each fault location and fault resistance the value of parameters has to be changed manually, the test has to be run and results have to be analysed (manually as well). Figure 2 shows what task has to be done for each of the tests.

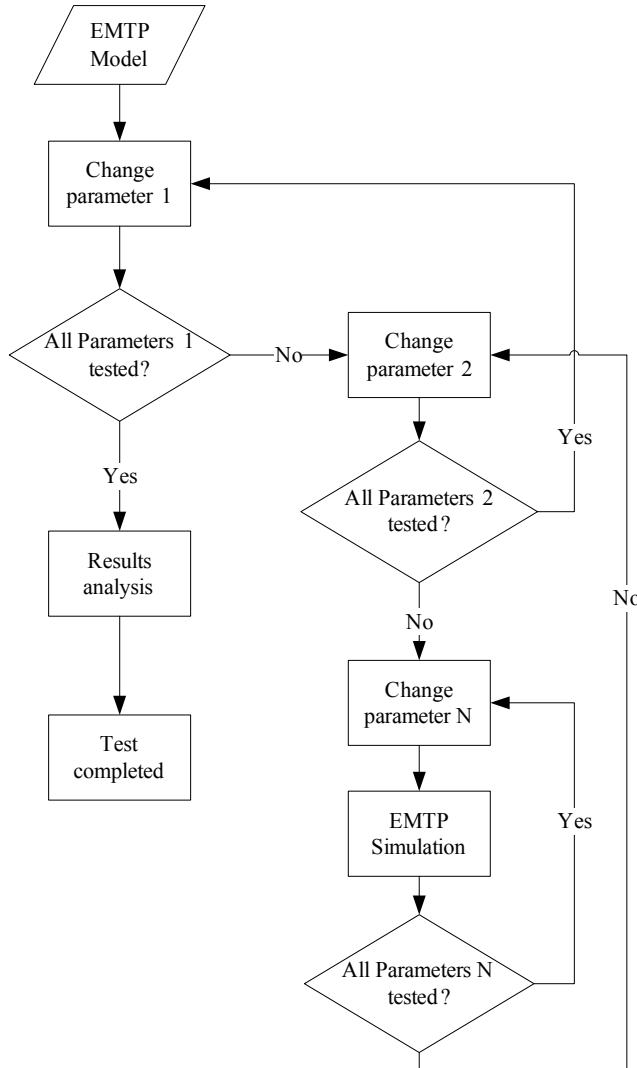


Fig. 2. Breakdown of tasks done during transient testing

Continuing with our example if it is required to simulate faults at 10 different locations with 3 different values of fault resistance and 3 different fault inception angles

this brings the total number of simulations to 90. It is easy to imagine scenarios which increase the number of simulations even further.

Conducting all those simulations manually is error prone and additionally if some changes have to be done to the system used for simulation all the scenarios have to be simulated again. All of this reduces the benefits of MBD.

Large parts of testing can be automated therefore making it easy to test against different fault scenarios. The following sections describe how EMTP simulations can be automated and how the waveforms can then be used to test Simulink based algorithms.

4.1. AUTOMATION OF ATP-EMTP TESTING

When a model of a power system is created in ATP-EMTP before it is actually simulated it gets translated into a format understandable for the EMTP solver. This

```

1 BEGIN NEW DATA CASE
2 C -----
3 C Generated by ATPDRAW July, Saturday 13, 2013
4 C A Bonneville Power Administration program
5 C by H. K. Høidalen at SEFAS/NTNU - NORWAY 1994-2009
6 C -----
7 C dT << Tmax >> Xopt << Copt >
8     1.E-6      .1
9     |500      1      0      0      0      0      0      1      0
10 $PARAMETER
11 RI =1 $$
12 LI =0.001 $$
13 CI =0 $$
14 R_____ =RI
15 L_____ =LI
16 C_____ =CI
17 BLANK $PARAMETER
18 C      1      2      3      4      5      6      7      8
19 C 34567890123456789012345678901234567890123456789012345678901234567890
20 /BRANCH
21 C < n1 >< n2 ><ref1><ref2>< R >< L >< C >
22 C < n1 >< n2 ><ref1><ref2>< R >< A >< B ><Leng><><>0
23 X0001AX0004A          R_____ L_____ C_____          1
24 X0001BX0004B          1. .001          1
25 X0001CX0004C          1. .001          1
26 /SOURCE
27 C < n 1><>< Ampl. >< Freq. ><Phase/T0>< A1 >< T1 >< TSTART >< TSTOP >
28 14X0001A      1.E4      50.          -1.      100.
29 /OUTPUT
30 BLANK BRANCH
31 BLANK SWITCH
32 BLANK SOURCE
33 BLANK OUTPUT
34 BLANK PLOT
35 BEGIN NEW DATA CASE
36 BLANK

```

Fig. 3. Example .ATP file

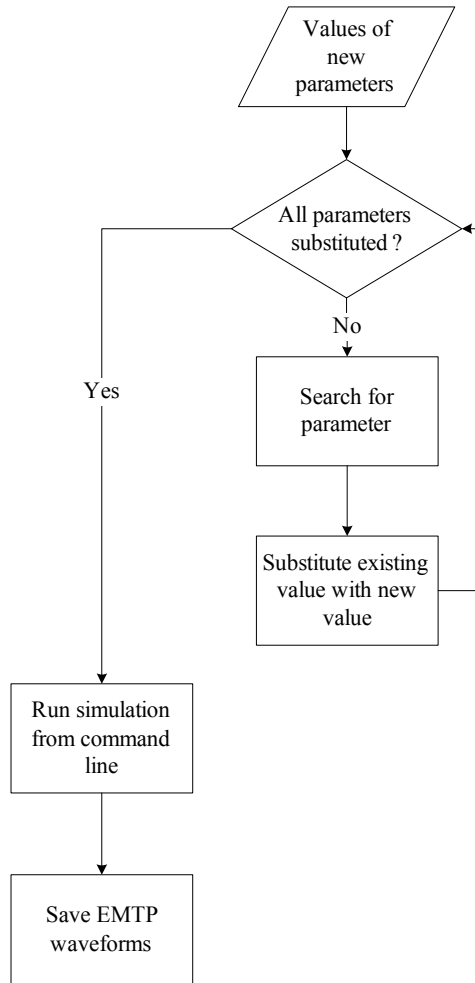


Fig. 4. Procedure for automation of EMTP testing

way a graphical. ACP file is converted into .ATP file which describes the circuit in a textual format. Normally when a single simulation is run the conversion is transparent to the user and there is no need to read the .ATP file unless there is a problem with the simulation.

The structure of an example .ATP file (consisting of one source and RLC element) is shown in Fig. 3. Details on how the file is structured can be found in [1].

As shown in Fig. 3 all parameters defined in the graphical tool can still be accessed in the textual file (lines 11 to 13). For each test the value of a parameter can be changed automatically by finding the name that was defined in ATP Draw. After the value is substituted the new .ATP file is used as an input to the EMTP solver.

The whole process can be easily controlled by Matlab script which would contain all the values for each of the parameters. At the end of each simulation the script would save the measurements for the particular simulation in a separate file so that waveforms can be stored and reused whenever required e.g. during regression testing.

Figure 4 shows the procedure that would have to be implemented using Matlab script.

Going back to the example of distance protection it is easy to write a script which will run a simulation for each combination of fault location, fault resistance and fault inception angle.

4.2. AUTOMATION OF SIMULINK MODEL TESTING

After an algorithm is designed in Simulink it is important to be able to thoroughly test it. One way of doing that is using waveforms generated by EMTP simulations as test vectors. For each of the tests a set of expected outputs needs to be created as well in order to be able to evaluate whether the function has operated correctly. In addition to functionally proving that the algorithm operates correctly in all simulated scenarios it is also important to assess how much of the model was actually tested.

If one takes again distance protection as an example one can have many tests which prove that the behaviour is correct for different fault locations, resistance and inception angles however we never tested whether the function can recognize that the voltage measured is not high enough to provide an accurate impedance calculation. If that feature has been implemented but one has not tested it then one needs a way of finding out about it.

This can be done using different types of model coverage. Some of the coverage types available in Simulink are decision coverage, condition coverage and modified condition-decision coverage. The detail of each of them can be found in [2] however each of them indicate how much of the implemented algorithm has actually been exercised during all the tests.

Testing automation can be achieved in Simulink using different techniques. The preferred technique is to load test vectors from a file into the Matlab workspace and run the Simulink models using them as an input. This way there is no need to create and maintain test harness as the model can be run on its own.

Depending on the type of test vector and the modelled function, there may be a need for additional pre-processing on the input signal. As described in Section 0 modelling can cover multiple domains therefore this pre-processing can include CT and ADC modelling as well as Fourier algorithm for calculating the magnitude and angle of the signal. Depending on the function this may or may not be the case as some functions can operate on raw samples.

Figure 5 shows the procedure of configuring the model to use data in Matlab workspace as input vectors.

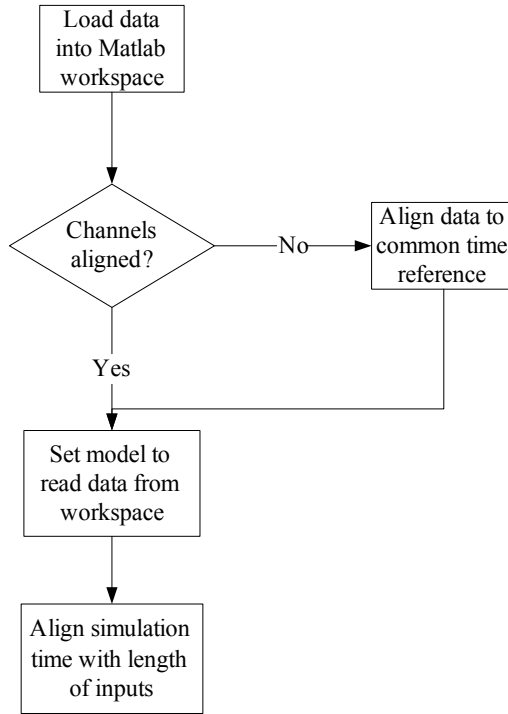


Fig. 5. Procedure for using workspace variables as inputs to Simulink model

When using data from the workspace Simulink requires that all inputs are synchronised to a common time reference. If this is not the case then some pre-processing of workspace variables will need to be done. In most cases a linear interpolation is sufficient but this depends on the sampling rate of the original data.

Since the parameters of a Simulink model can be changed using a Matlab script it is possible to run a whole set of tests by simply iterating through the files containing the input data. As long as the names of the variables in those files are consistent the number of tests can be increased.

This flexible approach allows Simulink models to be tested using data collected during relay operation (i.e. disturbance records) or results of a simulation.

5. IMPLEMENTATION AND TESTING OF UNDER FREQUENCY FUNCTION

Using the technique described in the previous section allows testing of any protection function. As an example for this paper an under frequency function was chosen since large variations of frequency are rarely observed on a real power system therefore not many disturbance records of such events are available.

Under frequency protection responds to a prolonged decrease of power system frequency. This is normally caused by mismatch between power supply and demand and can occur e.g. when a main link with another major part of the power system is disconnected.

Since the reduced frequency can have an adverse effect on both the electrical load and the generator supplying the system it is important to be able to detect the decrease of frequency.

The following equation describes the relationship between the change in real power, the total inertia of the system (H) and the corresponding change in frequency.

$$\Delta P = 2 \cdot H \cdot \Delta f \tag{1}$$

Although this can give an estimated value of frequency over time it only takes into account the inertia of the system without considering the response of the turbine which is important for evaluating the frequency over tens of seconds.

Figure 6 shows a Simulink block diagram of an under frequency function. Detailed description of Simulink and its features can be found in [3].

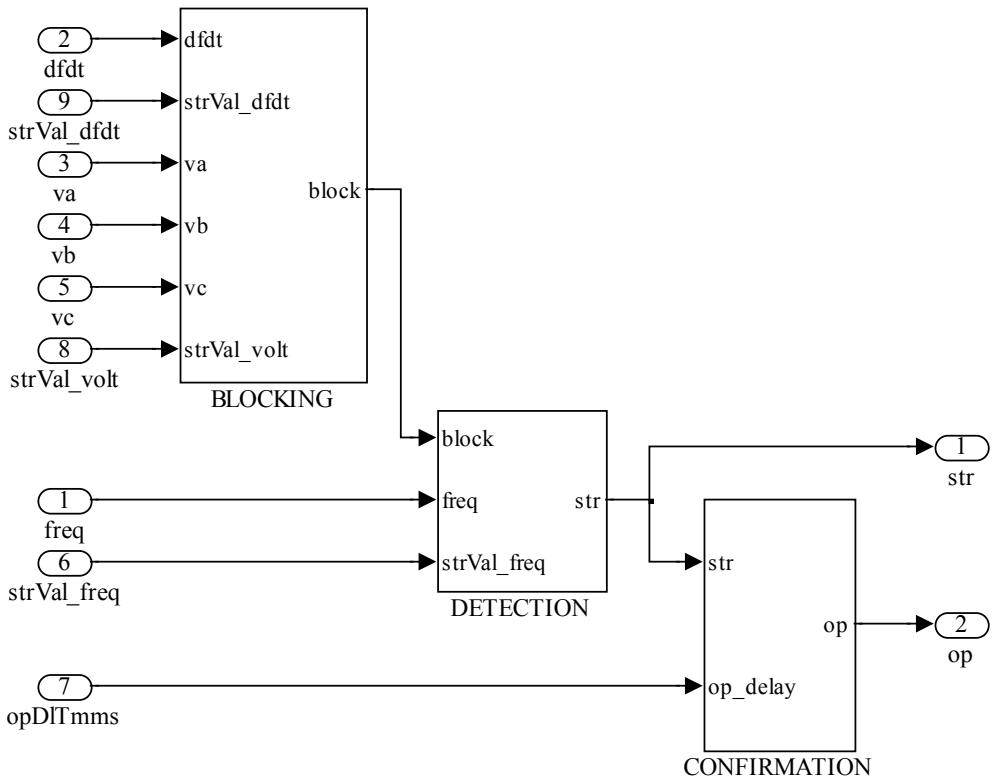


Fig. 6. Block diagram of under frequency function

The model consists of three main blocks:

- Under frequency detection where the measured value of frequency is compared to a threshold in order to determine if the function should operate. Also, any blocking signals are taken into account in this block.
- Under frequency confirmation where a certain time delay may be applied in order to make sure that the function will not operate for transient frequency excursions. The delay can normally be set by the user according to the specific application.
- Under frequency blocking where a decision is made whether protection needs to be blocked despite the frequency falling below the set threshold. One application scenario is when the magnitude of the voltage is so low that accurate measurement of frequency is impossible therefore the protection has to be blocked.

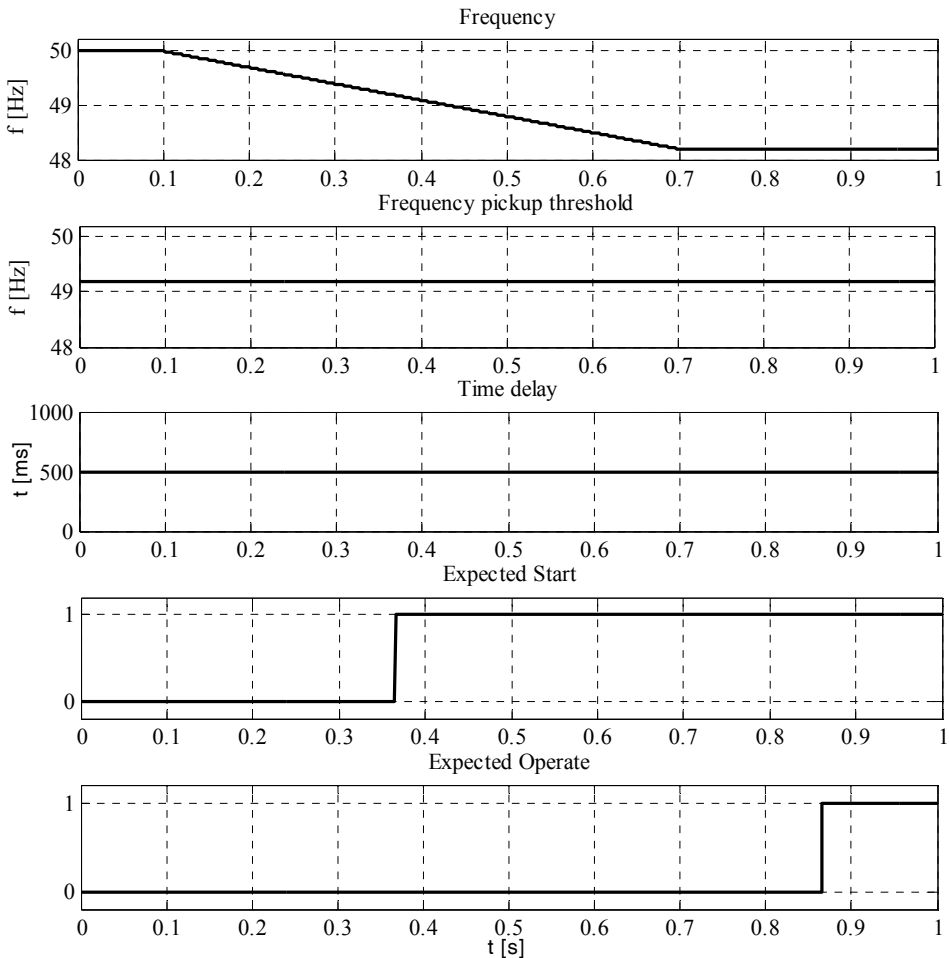


Fig. 7. Example of test vectors and expected results

Having the model designed in Simulink allows this behaviour to be tested. In this paper two types of tests are used. First the response of the function to ideal signals is tested which means that any errors due to the measurement of the frequency are ignored. Figure 7 shows example test vectors along with expected outputs. For the sake of clarity not all inputs are shown. The test vectors shown are used as inputs to the model. Expected outputs are compared with the outputs of the function after the execution of the test – the comparison can easily be implemented as a simple Matlab script. In this example a 3 Hz/sec frequency ramp is applied with the under frequency setting of 49.2 Hz. The Start output is expected to be asserted at 0.36 sec and the Operate output is expected to follow the Start with a 500 ms delay.

The aim of the test shown above is to prove that the algorithm works as required for ideal signals and not to establish whether the function will operate correctly in real world applications. The latter can be done using the second type of testing which uses power system waveforms – in this case results of EMTP simulations. This test not only mimics the behaviour of the power system but also introduces errors that exist in real products, e.g. nonlinearity of current transformer (CT) and analog-to-digital converter (ADC) as well as inaccuracies added due to the measurement technique. Depending on the required accuracy of the simulation some of the mentioned sources of errors can be ignored or some other additional errors can be added. Additional information on the subject can be found in [4].

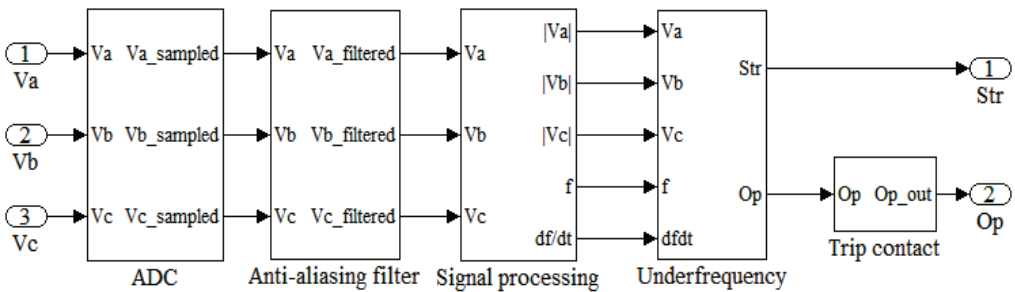


Fig. 8. Simulink model including the whole acquisition chain

Figure 8 shows the Simulink model used in these tests (for the sake of clarity all the settings were hidden). Comparing to the model from Fig. 6 additional blocks are present in order to bring the model as close to reality as possible. Starting from the left the ADC is modelled in order to take into account its dynamic range. Following the sampling of the voltage waveforms anti aliasing filtering is applied. The next block is responsible for signal processing of raw samples and producing frequency and voltage measurements. Depending on the type of filtering used this block can introduce significant delay into the total operating time of the function therefore it is important to

model it accurately. The next block is the under frequency logic. The last block on the right represents the delay introduced by the relay contacts which adds to the total delay of the under frequency function.

The EMTP model used as the source of the test vectors are shown in Fig. 9 and Fig. 10. It consists of two synchronous machines connected via a transformer and a line. One of the machines represents a 10MVA small local generation which normally exports real power into the system. The generator itself is not able to provide power for all local loads therefore if the circuit breaker (CB) at the common coupling point is opened the frequency of the islanded system will decrease which should cause the under frequency function to operate.

On the other hand the under frequency function should not operate for transient frequency dips caused by faults on the system (in our case represented as a fault on the line connecting the small generator with the rest of the power system).

The third scenario to be considered is when the frequency relay is connected at a substation powering large induction motors. When a fault on the system causes the substation to become isolated from the supply for a short period of time the motors work as generators producing fast decaying voltage with decreasing frequency. It is required for the frequency protection not to operate during such a scenario.

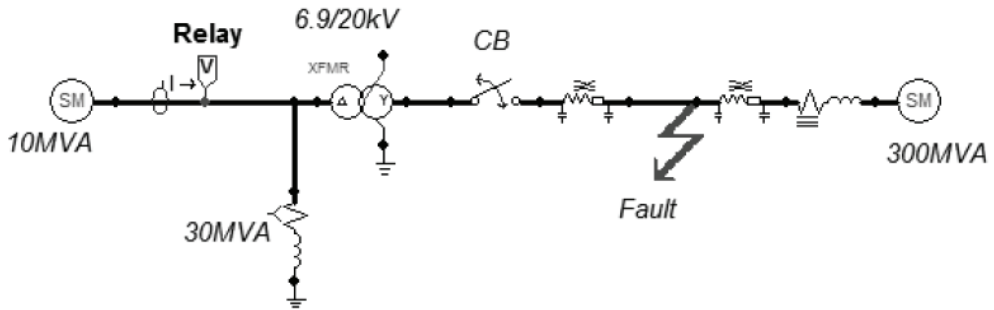


Fig. 9. Interconnection between distributed generation and the grid

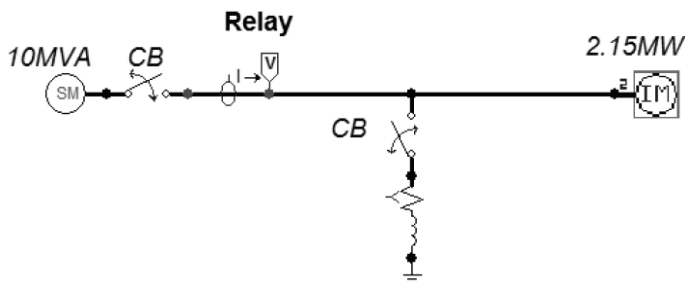


Fig. 10. Generator powering an induction motor

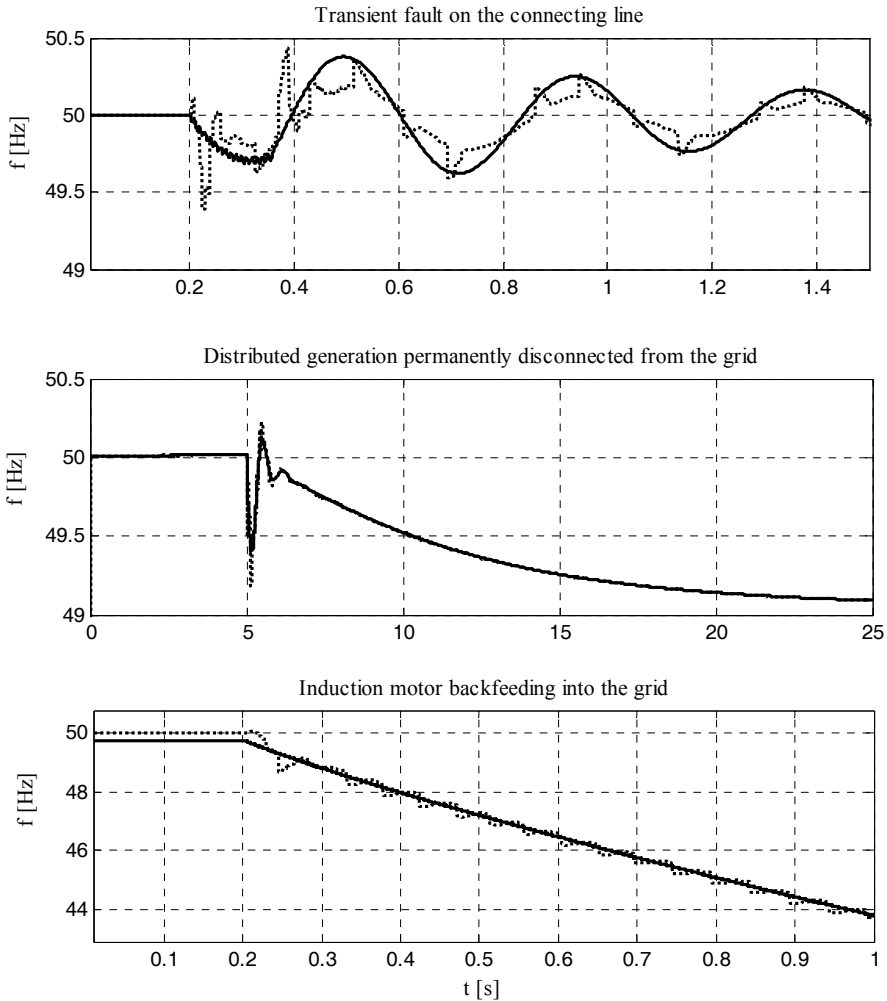


Fig. 11. Waveforms for each of the test scenarios (solid line – actual, dotted line – measured frequency)

Figure 11 shows example results for each of the test cases described. Both the measured and actual frequencies are plotted in order to show the differences. Depending on the algorithm used for frequency measurements the error can vary. This allows selecting the best suited algorithm. When the frequency measurements are used as inputs for under frequency it also allows determining whether the relay would behave correctly in the particular scenario.

Each of the diagrams in the above figure shows both measured and actual frequencies. The measured frequency is obtained using the signal processing block and therefore is dependent on the algorithm used. The actual frequency is calculated based on

the rotation speed of the rotor of synchronous generator or induction machines (depending on the test scenario). Ideally both the actual and the measured frequency should be identical however due to inaccuracies of the processing chain and delays introduced by the filter algorithms a small difference can exist. The difference varies depending on the test scenario therefore automated testing is ideal for choosing the most suitable algorithms.

Waveforms gathered during EMTP simulation are be used as input to the Simulink model as described in 4.2. This allows checking whether the settings selected for the frequency relay will work as expected for all the simulated disturbances.

6. CONCLUSIONS

This paper demonstrated how available CAD tools can be used to design and test power system protection functions. By following the described workflow it is possible to create new protection functions by using blocks of functionality provided by Simulink. A design can be first tested to prove that the function works for ideal signals. In addition Simulink allows gathering of model coverage metrics which can demonstrate that the function was tested thoroughly. The final stage of testing is by using waveforms generated using ATP-EMTP. Using the method described in the paper it is possible to simulate multiple scenarios automatically. Since all the tests can be stored and easily re-run it is very easy to conduct regression testing or identify problems with the design. By modelling the parts of hardware used to run the protection function on it is possible to make the simulation results even closer to those of a physical protective relay.

The under frequency example shows the benefits of testing the function using ATP-EMTP generated waveforms in conjunction with Simulink. By simulating multiple scenarios one can gain confidence that the protection function will operate as expected and because it is easy to extend the list of test cases one can easily check whether the function meets the new application requirements.

REFERENCES

- [1] PRIKLER L., HOIDALEN H.K., *ATPDraw User's Manual version 5.6*, 2009.
- [2] BARESEL A., CONRAD M., SADEGHIPOUR S., WEGENER J., *The interplay between model coverage and code coverage*, EuroSTAR Software Testing Conference 2003.
- [3] MATHWORKS, *Simulink User's Guide*.
- [4] GEC MEASUREMENTS, *Network protection and automation guide 3rd Edition*, 1987.

Tahir LAZIMOV*, Esam SAAFAN**

TRANSITIONAL PROCESSES AT SWITCHING-OFF UNLOADED POWER TRANSMISSION LINES BY MODERN CIRCUIT-BREAKERS AND THEIR COMPUTER SIMULATION

The article presents results of transitional processes' computer simulation at switching-off unloaded power transmission line of rated voltage 220 kV by auto-compression (SF6) circuit-breakers. Transitional voltages (voltage across the line terminals and recovery voltage) at switching-off were calculated and studied in the research carried out. There was also considered dependence between transitional voltages' magnitudes and power transmission lines lengths. There were studied some computational peculiarities of the problem under consideration. In particular, the numbers of pi-sections provided satisfactory adequacy of lines' equivalency at computer simulation for their typical lengths were determined. There were also estimated optimum simulation parameters provided stability of transitional regime parameters.

1. INTRODUCTION

Switching-off power transmission lines is well-studied transitional process for power electric systems [1, 2].

There is a common peculiarity for all the kinds of transitional processes at their computer simulation conditioned by possible losing of transitional regime parameters' (voltages and currents in the present research) stability. It takes place because of so called "stiffness" of differential equations' solutions and rounding errors accumulation [3,4]. It is especially important matter for computer simulation of transitional processes having high steepness e.g. switching-off electric current in mediums with great electric strength such as vacuum or highly-pressed SF6. Arc quenching in such

* Electric Supply and Insulation Chair, Azerbaijan Technical University, AZ1009, Baku, Azerbaijan, tahirlazim@gmail.com

** Faculty of Engineering, University of El-Mansoura, Box 35516, Mansoura, Egypt, esam_ali_saafan@yahoo.com

mediums is accompanied with steep splashes of recovery voltages. From the computational point of view it means increasing of instantaneous values of voltages and corresponding growth of rounding's local errors.

Computer simulation of transitional processes in power transmission lines brings another one characteristic in research. It is necessary to determine number of pi-sections modeling transmission line provided satisfactory tolerance at scheme transformation [5]. This number may depend on some factors such as power transmission line's rated voltage, length and also some geometrical dimensions and sizes of towers and phase conductors. In other words, it directly depends on free frequency of transitional process, line length and electromagnetic waves' propagation speed along the line [6].

2. COMPUTATIONAL GROUND

An electrical connection scheme and corresponding equivalent network of unloaded 220 kV power transmission line are presented in the Fig. 1.

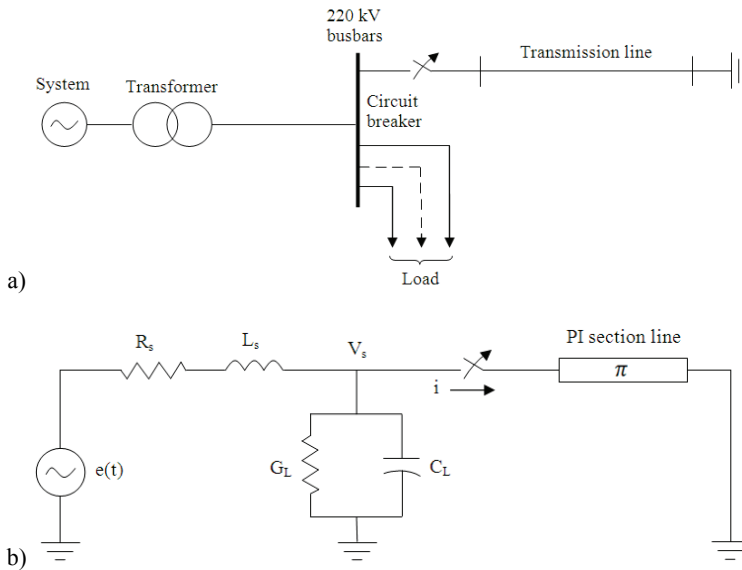


Fig. 1. Switching-off power transmission line:
a) electrical connection scheme; b) equivalent network

The following denotations are used in the Fig.1:

- $e(t)$ is system's e.m.f.;
- R_s and L_s are correspondingly resistance and inductance of the equivalent system the line considered connects to;

- G_L and C_L are correspondingly conductivity and capacitance of the substation 220 kV busbars' load;
- V_s is voltage of the line on the system side;
- pi-sectioned line is the equivalent network for the 220 kV's transmission line of given length.

The following per unit parameters of 220 kV's power transmission line were used [7]:

- resistance $R_o = 0.08$ Ohm/km;
- inductance $L_o = 1.31$ mH/km;
- capacitance $C_o = 8.79$ nF/km.

The switching-off processes were researched at case of use auto-compression (SF6) circuit-breaker. It was modeled by its chopping current determined depending on magnitude of switched-off current in accordance with [8] and electrical strength restoration law which in accordance with [9,10] is the cosine one.

For computer simulation of 220 kV's power transmission line's switching-offs we used the MATLAB ordinary differential equation (ode) solvers especially ode 23tb method and some others (ode 23t and ode 15s) [5,11].

The optimum parameters of computer simulation were determined by the condition to obtain stable solutions of the differential equations formalized transitional voltages and currents as it was done e.g. in [11, 12, 13]. It is widely known that possible loosing of stability is conditioned by "stiffness" of the differential equations related transitional voltages and currents with their first temporal derivatives [3, 14]. "Stiff" differential equations are sensitive to unavoidable accumulation of rounding errors may cause loosing of stability.

Further stability of the problem under consideration will be estimated.

3. RESULTS OBTAINED AND DISCUSSION

In the Fig.2, Fig.3 and Fig.4 the curves of transitional voltages (on the 220 kV busbars, on the line's input and recovery one) at use computer simulation for the number of pi-sections $N = 1$ and lines length's 80, 120 and 160 km are presented.

In accordance with [2] aerial power transmission lines of lengths less than 150–250 km can be presented by only pi-section i.e. line parameters' distribution may not be taken into account. It means neglecting of wave character of transitional processes for minded lengths and use of lumped parameter's model. In general expediency of taking into account distributed parameters must be estimated by comparison of length corresponded to the greatest natural frequency with the length of considered line.

As it is seen from the Fig. 2, Fig. 3 and Fig. 4 the natural frequencies for the lines of lengths 80, 120 and 160 km are correspondingly equaled 1175, 850 and 620 Hz.

The wave lengths are equaled about 254, 353 and 483 km in the same correspondence (determined as a ratio of electromagnetic waves propagation speed and natural frequency).

On the other hand there is another way to estimate the number of pi-sections needed for the line equivalent representation given in [6]. As it is shown in [6] the number of pi-sections used relates with the maximum frequency by the following expression,

$$f_{\max} = \frac{N\varrho}{8l'} \quad (1)$$

where $\varrho = (L_o C_o)^{-0.5}$ is electromagnetic waves' propagation speed along the line; l' is length of line.

The minded velocity for the line under consideration is equaled to 294693 km/s. Then the maximum number of pi-sections for the lines of lengths 80, 120 and 160 km will be equaled to 2.55, 2.77 and 2.69 correspondingly. It means that in accordance with [6] the number considered may be taken as 1 or 2.

Note that simulation results presented in the Figs. 2, 3 and 4 were obtained at use the ode 23tb method for initial step size 100 nanoseconds and tolerance 10^{-7} .

Let us now consider simulation at use the number of pi-sections more than 1. Research carried out had shown that results of computer simulation at different numbers of pi-sections may distinguish seriously enough. E.g. difference between magnitudes of transitional voltages across the line terminals at $N = 1, 2$ and 3 may reach 48%, difference between transitional recovery voltages – 20%. Moreover, there is not any regularity between calculated transitional voltages and the number of pi-sections used.

In the Fig. 5 and Fig. 6 are presenting curves of transitional voltages obtained at computer simulation switching-off 220 kV's power transmission line of length 120 km by SF6 circuit-breaker for number of pi-sections 2 and 3. Comparing these curves with ones presented in the Fig. 3 (i.e., for the same line at $N = 1$) we can see that the high-frequency oscillations appearing in the cases of use different numbers of pi-sections is distinguished enough. It has no any physical meaning because just only natural frequency may characterize real line with no connections between circuit-breakers installed on its edges. Obviously the oscillations seen in the Fig. 5 and Fig. 6 (unlike ones in the Fig. 3) have calculative nature and causes by dividing line's length at pi-sectioning.

The power transmission lines of rated voltages higher than considered one may have greater lengths and correspondingly less natural frequency. Our research has shown that for the longer lines pi-sectioning at more than 1 section may be more expedient. Remind that historically lines' pi-sectioning was worked up for steady-state regimes. Increasing line's length is a kind of approaching the line's natural frequency to the standard one.

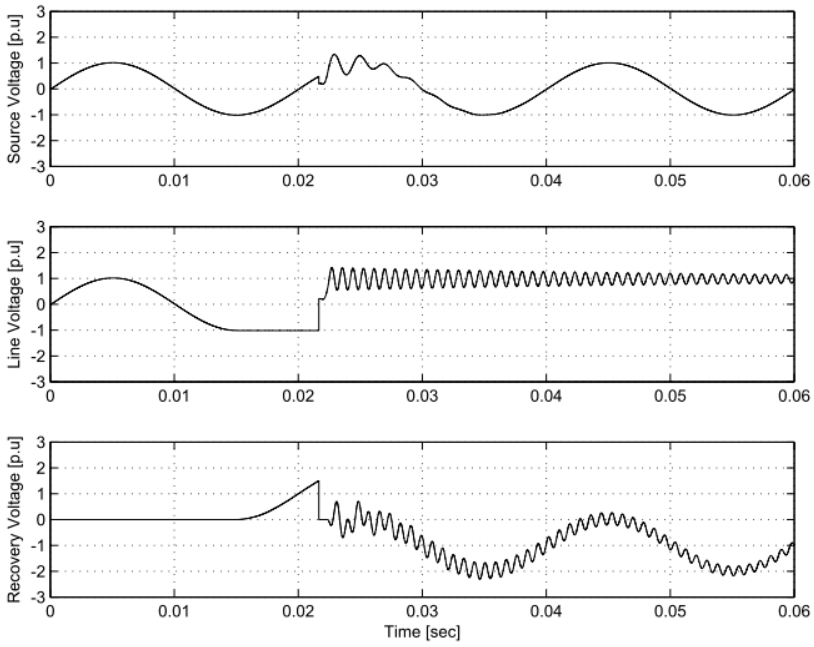


Fig. 2. Transitional voltages at line length 80 km, $N = 1$

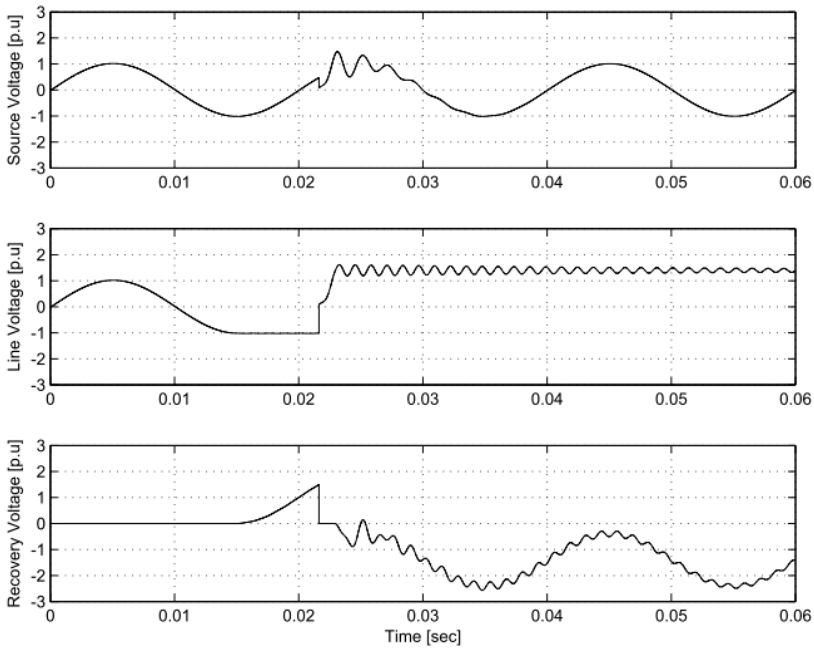


Fig. 3. Transitional voltages at line length 120 km, $N = 1$

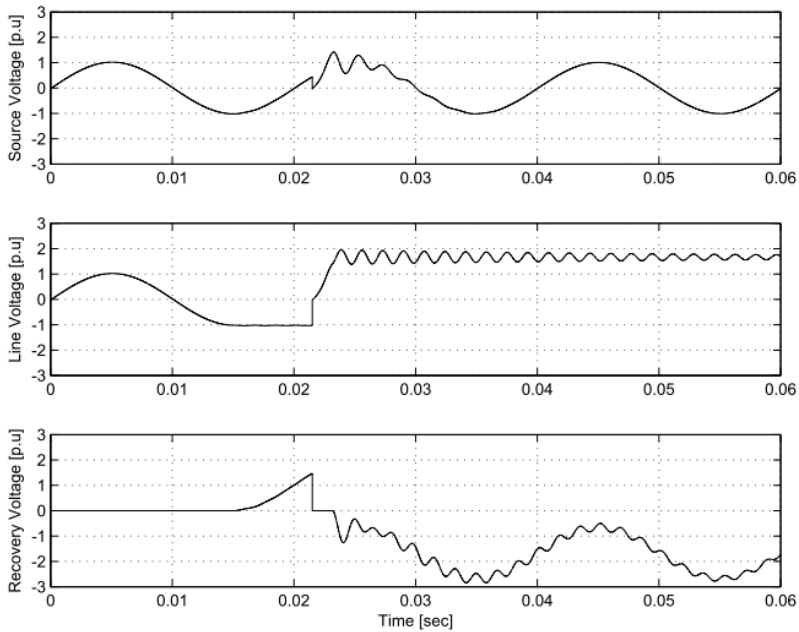


Fig. 4. Transitional voltages at line length 160 km, $N = 1$

Analyzing Fig. 2, Fig. 3 and Fig. 4 from the point of view transitional voltages' magnitudes we can state that switching-off unloaded 220 kV power transmission lines by SF6 circuit-breakers does not cause appearance of voltages on lines' terminals more than allowable one. In the same time recovery voltages across the circuit-breakers' poles may prevail above allowable grade for relatively long lines.

4. ON STABILITY

In the present research the ode 23tb method was mainly used. While carrying out the research we had stated that it was possible to get stable solutions for all the transitional voltages just at initial step sizes no more than 100 nanoseconds in wide range of tolerances minded above. Note that at computer simulation the problems of switching-off capacitor banks and unloaded power transmission lines [11, 15] we got sometimes stable solutions at greater initial step sizes. It means that the problem of computer simulation the switching-offs unloaded power transmission lines is sensitive enough to changes of initial step size.

We have also noticed that increasing the number of pi-sections leads to worsening of stability. It takes place because of additional contribution in global error brought by artificial calculations conditioned by power transmission line pi-sectioning at $N > 1$.

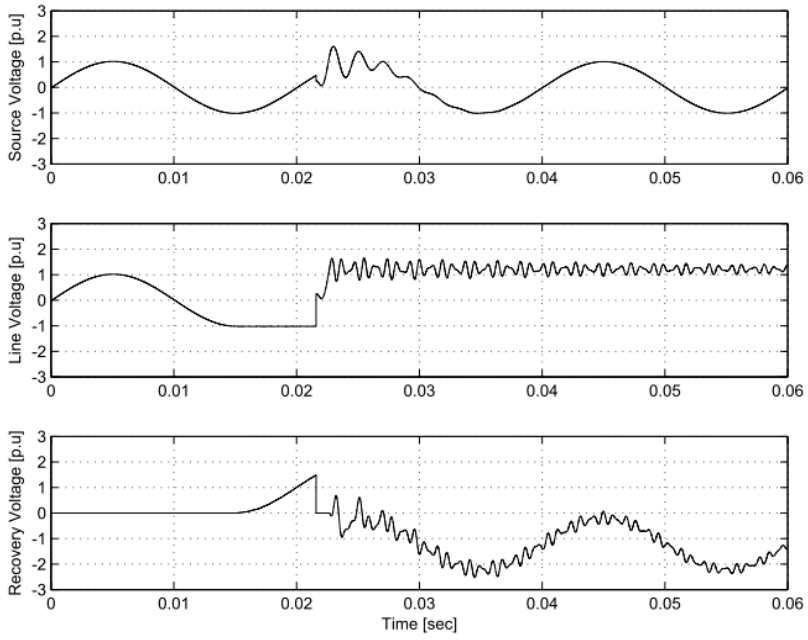


Fig. 5. Transitional voltages at line length 120 km, $N = 2$

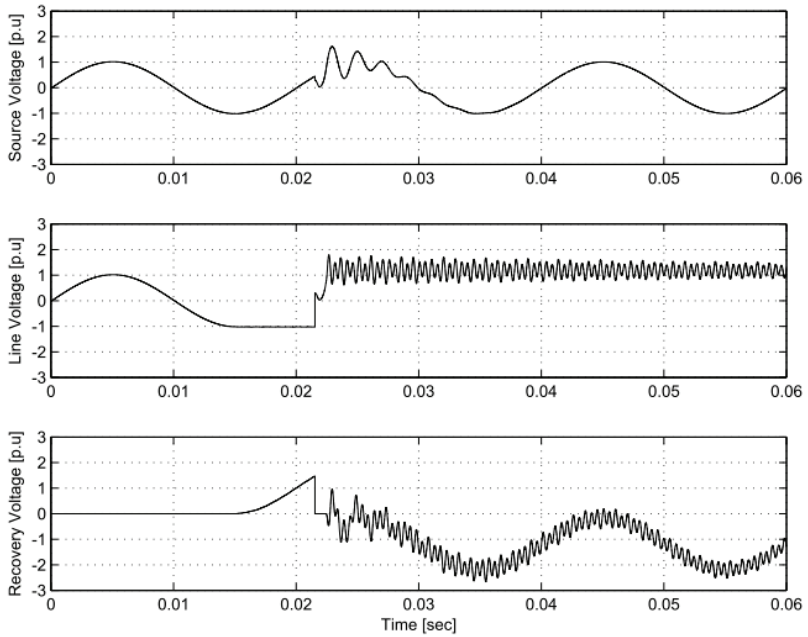


Fig. 6. Transitional voltages at line length 120 km, $N = 3$

5. CONCLUSIONS

Transitional voltages across the terminals at switching-off unloaded 220 kV power transmission lines by SF6 circuit-breakers do not exceed the allowable value of this insulation grade. Transitional recovery voltages at the same switching may exceed the minded grade for longer lines.

As a rule transitional voltages have greater values for longer lines. It may be explained by approaching the current chop instant to the current zero for longer lines. As a result current interruption takes place at greater angle between switched-off current and voltage phasors (closer to 90 degrees). It means appearance of a greater magnitude of voltage across the line terminals at the current chop instant.

Relatively little (in comparison with wave length corresponded to natural frequency) length of 220 kV power transmission lines lets to present their equivalent network with just only pi-section at computer simulation switching-off transient. Use of greater number of pi-sections is not expedient because that it causes artificial oscillations of transitional voltages conditioned by the dividing of line by shorter sections had free frequencies more than line's natural frequency. These artificial oscillations distort curves and magnitudes if transitional voltages.

REFERENCES

- [1] BICKFORD J.P., MULLINEUX N., REED S.R., *Computation of Power System Transients*, Peter Peregrinus, Ltd., England, 1976.
- [2] RAZEVIK D.V., *High Voltage Engineering*, Khanna Publishers, Delhi 1972.
- [3] SHAMPINE L.F., *Numerical Solutions of Ordinary Differential Equations*, Chapman and Hall, New York 1994.
- [4] HAIRER E., NORSETT S.P., WANNER G., *Solving Ordinary Differential Equations*. Part 1, Springer-Verlag, Berlin, Heidelberg, New York, London, Paris, Tokyo 1987.
- [5] LAZIMOV T.M., IMANOV S.V., *Some results of unloaded line switching-offs' computer simulation*. Proceedings of the ELECO '2007 International Conference, Bursa, Turkey, 2007, 147–150.
- [6] <http://www.mathworks.com/help/physmod/powersys/ref/pisectionline>
- [7] BAUMSTEIN I.A., BAJANOV S.A., *High Voltage Electrical Installations*, Energoatomizdat, Moscow, 1989 (in Russian).
- [8] RUBEN D. GARZON, *High voltage circuit breakers design and applications*, Marcel Dekker, New York 2002.
- [9] LAZIMOV T.M., AKHUNDOV S.A., *Modeling of electrical strength of high voltage circuit-breakers*. Proceedings of the International Symposium SIEMA '2001, Kharkov, Ukraine, October 18–20, 2001, 112–114 (in Russian).
- [10] AKHUNDOV S.A., Abstracts of Ph.D. Thesis, Baku 2002.
- [11] LAZIMOV T.M., SAAFAN E.A., *On interaction between circuit-breaker and network at small inductive currents switching-offs*, Present Problems of Power System Control, No. 1, Wrocław, Poland, 2011.

- [12] LAZIMOV T.M., IMANOV S.V., *On stability while simulating the switching-offs the capacitive and small inductive currents*. Proceeding of the MEPS '06 International Symposium, Wrocław, Poland, Sep. 2006, 407–410.
- [13] SAAFAN E.A., Abstracts of Ph.D. Thesis, Baku 2012.
- [14] LAZIMOV T., AKHUNDOV S., *Peculiarities of transients' simulation in electrical circuits*. Proceedings of the Republican Conference on IT, Baku, Azerbaijan, 2003 (in Russian).
- [15] LAZIMOV T., IMANOV S., SAAFAN E.A., *Transitional Recovery Voltages at Capacitive Currents Switching-off's by Vacuum and SF6 Circuit-Breakers*, Energy and Power Engineering, Vol. 6, No. 5, Chicago, USA, 2012.

